Utility of natural and artificial geochemical tracers for leakage monitoring and quantification during an offshore controlled CO₂ release experiment

Anita Flohr [a],[*], Juerg M. Matter [a], Rachael H. James [a], Kevin Saw [b], Robin Brown [b], Jonas Gros [c], Stephanie Flude [d], Christopher Day [d], Kate Peel [b], Douglas Connelly [b], Christopher R. Pearce [b], James A. Strong [b], Anna Lichtschlag [b], Darren J. Hillegonds [d], Christopher J. Ballentine [d], Rebecca L. Tyne [d]

[a] *School of Ocean and Earth Science, National Oceanography Centre Southampton, University of Southampton Waterfront Campus, European Way, Southampton SO14 3ZH, United Kingdom*
[b] *National Oceanography Centre, European Way, Southampton SO14 3ZH, United Kingdom*
[c] *GEOMAR Helmholtz Centre for Ocean Research Kiel, Wischhofstr. 1-3, 24148 Kiel, Germany*
[d] *University of Oxford, Department of Earth Sciences, South Parks Road, Oxford OX1 3AN, United Kingdom*

ARTICLE INFO

ABSTRACT

To inform cost-effective monitoring of offshore geological storage of carbon dioxide (CO₂), a unique field experiment, designed to simulate leakage of CO₂ from a sub-seafloor storage reservoir, was carried out in the central North Sea. A total of 675 kg of CO₂ were released into the shallow sediments (~3 m below seafloor) for 11 days at flow rates between 6 and 143 kg d^{-1}. A set of natural, inherent tracers (^{13}C, ^{18}O) of injected CO₂ and added, non-toxic tracer gases (octafluoropropane, sulfur hexafluoride, krypton, methane) were used to test their applicability for CO₂ leakage attribution and quantification in the marine environment. All tracers except ^{18}O were capable of attributing the CO₂ source. Tracer analyses indicate that CO₂ dissolution in sediment pore waters ranged from 35 % at the lowest injection rate to 41% at the highest injection rate. Direct measurements of gas released from the sediment into the water column suggest that 22 % to 48 % of the injected CO₂ exited the seafloor at, respectively, the lowest and the highest injection rate. The remainder of injected CO₂ accumulated in gas pockets in the sediment. The methodologies can be used to rapidly confirm the source of leaking CO₂ once seabed samples are retrieved.

1. Introduction

The atmospheric carbon dioxide (CO₂) concentration has risen from 277 parts per million (ppm) in pre-industrial times to ~412 ppm in 2020 (Friedlingstein et al., 2019; Dlugokencky et al., 2020). In 2016, the United Nations Framework Convention on Climate Change (UNFCCC) agreed to take actions to keep global warming below 2 °C above the pre-industrial level. Integrated Assessment Models of different mitigation strategies suggest that decarbonisation pathways consistent with the 2 °C target rely on large-scale greenhouse gas removal from the atmosphere (IPCC, 2018), which involves the direct or indirect removal of CO₂ from the atmosphere, or so-called 'negative emissions'. Several technologies have the potential to achieve negative emissions including direct air capture (DAC) and bioenergy with carbon capture and storage

(Haszeldine et al., 2018). Carbon capture and storage (CCS) involves the capture of CO₂ from large point sources, such as industrial power plants, or directly from the atmosphere, and its injection into geological storage reservoirs such as deep saline aquifers or depleted oil and gas reservoirs for permanent storage (IPCC, 2005).

Suitable geological formations for CO₂ storage exist onshore and offshore although onshore storage can be restricted, e.g., by the need to avoid large population centres and protection of potable groundwater resources (Lee et al., 2014; Ringrose and Meckel, 2019). The majority of Western Europe's potential CO₂ storage capacity is located offshore, mainly in the North Sea (IEAGHG, 2008; Vangkilde-Pederson, 2009). There are a small number of active (Sleipner, North Sea, Norway; Snøhvit, Barents Sea, Norway) and completed (K12-B, North Sea, Netherlands) offshore CO₂ injection projects in Europe that provide

confidence in the security of offshore CO_2 injection and storage (Furre et al., 2017; Hansen et al., 2013; Ringrose and Meckel, 2019; Van der Meer, 2013; Vandeweijer et al., 2011). However, CCS has yet to be implemented on an industrial scale. One of the barriers to large-scale CCS deployment in an offshore environment is the need to ensure that an unintended leakage of the injected CO_2 can be detected and managed. Leakage of injected CO_2 from well-selected and managed geological storage sites back into the atmosphere is generally considered unlikely (IPCC, 2005; Alcalde et al., 2018), and CO_2 storage integrity and effective monitoring of depleted gas fields has been demonstrated (e.g., Furre et al., 2017; Jenkins et al., 2012). However, effective environmental monitoring strategies are required to comply with international marine legislation (e.g., the EU CCS Directive (EU, 2009), the London Protocol (IMO, 2006), the OSPAR Convention (OSPAR, 2007) and to obtain public acceptance to operate (Mabon et al., 2015; Mabon et al., 2017; Mabon et al., 2014).

In the event of CO_2 leakage in the marine environment, CO_2 may partly or completely dissolve in sediment pore waters before entering the water column. When CO_2 dissolves in water, it reacts to form carbonic acid (H_2CO_3) that subsequently dissociates with release of H^+ to form bicarbonate (HCO_3^-) and carbonate (CO_3^{2-}) ions. The sum of the concentrations of these three species ($H_2CO_3 + HCO_3^- + CO_3^{2-}$) defines the dissolved inorganic carbon (DIC) content of the water (Zeebe and Wolf-Gladrow, 2001). Detecting and quantifying a release of CO_2 in the marine environment is challenging because CO_2 is naturally produced by biogeochemical processes such as the degradation of organic carbon and the dissolution of carbonate. Natural variations in DIC (e.g., tidal, seasonal) need to be distinguished from changes caused by a leak from a CCS reservoir; this can be difficult when the leak is small or the natural variability in baseline DIC is large (Blackford et al., 2017).

Chemical tracers that fingerprint the leakage of CO_2 from a storage reservoir can be effective tools for distinguishing between natural and leakage signals. A tracer is a non-toxic marker species that is either naturally present (inherent) in CO_2 or the reservoir or can be purposefully added to the injected CO_2 (e.g., Flude et al., 2016; Roberts et al., 2017). Ideally, tracers should be detectable at very low concentrations and have a low background concentration or a significantly different isotopic signature from that found in the environment. A variety of tracers have been proposed for CCS and tested as part of CO_2 injection and release experiments and in pilot CCS projects (Jenkins et al., 2015; Myers et al., 2013). To date, tracers have mainly been used for in-reservoir monitoring and characterisation, for validating the presence of injected CO_2 in the reservoir and to understand CO_2 migration pathways. Stable isotopes of carbon (^{13}C) and oxygen (^{18}O) have been applied successfully for in-reservoir monitoring of CO_2, for example for tracking the migration of the injected CO_2 gas, for quantifying the amount of CO_2 sequestered in the reservoir and for studying interactions between reservoir fluids and rocks (e.g., Khararka et al., 2006; Serno et al., 2016; Gilfillan et al., 2014; Györe et al., 2017; Györe et al., 2015; Assayag et al., 2009), as well as leakage monitoring (e.g., Kim et al., 2019; Schacht and Jenkins, 2014; Jones et al., 2014). Artificial tracers, such as sulfur hexafluoride (SF_6), perfluorocarbons (PFCs) and noble gases, have also been applied successfully to detect CO_2 breakthrough in terrestrial storage reservoirs (e.g., Boreham et al., 2011; Jenkins et al., 2015; Matter et al., 2016; Stalker et al., 2015) and leakage monitoring (e.g., Myers et al., 2019; Rillard et al., 2015; Nimz and Hudson, 2005). However, most tracer studies have been performed in onshore settings and the applicability of tracers in offshore marine environments and their behaviours in the marine environment are currently poorly understood (Roberts et al., 2017).

This study builds on the QICS (Quantifying and Monitoring Potential Ecosystem Impacts of Geological Storage) project, which completed the first controlled CO_2 release experiment in a marine setting. Leakage of injected CO_2 was detected through analysis of $\delta^{13}C$ of sediment pore waters, which reflected the $\delta^{13}C$ value of the injected CO_2 (Lichtschlag et al., 2015). Approximately 85 % of the injected CO_2 was estimated to

have remained in the sediment, both in gas pockets and dissolved in sediment pore water, but their relative proportions could not be verified (Blackford et al., 2014; Taylor et al., 2015; Cevatoglu et al., 2015). In order to better resolve the fate of CO_2 the use of inert tracers was recommended (Blackford et al., 2015).

To demonstrate the application of new and established methodologies for marine environmental monitoring of offshore CO_2 storage sites, the Strategies for Environmental Monitoring of Marine Carbon Capture and Storage (STEMM-CCS) project carried out a controlled CO_2 release experiment in the central North Sea (Flohr et al., 2021). For the first time, a set of natural, inherent tracers (^{13}C, ^{18}O) and non-toxic, added tracer gases (octafluoropropane (C_3F_8), sulfur hexafluoride (SF_6) and krypton (Kr)) were tested in a marine environment for their applicability for source attribution and leakage rate quantification at the seafloor. This paper summarises the key insights on tracer behaviour, sampling and analyses provided by the release experiment, and evaluates the utility of tracers for marine environmental monitoring of offshore CO_2 storage sites.

2. Materials and methods

2.1. CO_2 release experiment

The STEMM-CCS CO_2 release experiment was carried out near the proposed Goldeneye CO_2 storage reservoir, a depleted gas condensate field located offshore Scotland in the Outer Moray Firth, in the UK sector of the central North Sea (56–60 ̊N) (Dean and Tucker, 2017).

The field experiment took place between 27 April and 27 May 2019 and involved two research vessels: the UK royal research ship RRS *James Cook* (expedition JC180; Connelly, 2019) and the German research vessel RV *Poseidon* (expedition POS534; Schmidt, 2019). In brief, CO_2 gas and tracer gases were injected into the shallow sediment overburden (at a depth of ~3 m below seafloor (mbsf), total water depth 119 m) over a period of 11 days. The injection rate was increased in a series of steps over the course of the experiment (6, 14, 29, 86 to 143 kg CO_2 d^{-1}). A detailed description of the release site and the release experiment can be found in Flohr et al. (2021).

The CO_2 and tracer gases were injected into the shallow sediment via a gas release pipe that was connected to a custom-built gas storage and delivery system. The delivery system consisted of a pair of bulk CO_2 storage tanks (City Gas EOOD, Stara Zagora, Bulgaria), four manifolded bladder accumulators (QHP, England) that contained the concentrated tracer mixture, and a gas control unit. All of this equipment was mounted in a steel deployment frame (5.5 m length, 2.55 m width, 2 m height) that had a gross weight of 13 t (including a total of 3.3 t of liquid CO_2).

2.2. Geochemical tracers

Tracer gases were selected based on (i) previous work (Roberts et al., 2017; Myers et al., 2013 and references therein; Flude et al., 2016; Dean and Tucker, 2017), (ii) the underlying experimental setup, (iii) the physico-chemical properties of the tracers and (iv) aspects of availability, analytical feasibility and associated costs. The selected tracers were a set of inherent, natural ($\delta^{13}C$, $\delta^{18}O$) and added (C_3F_8, SF_6, Kr) tracers. In addition, the injected CO_2 gas naturally contained CH_4.

Other tracers such as trifluoromethyl sulfur pentafluoride (SF_5CF_3), xenon isotopes ([124,129]Xe), deuterated methane (CD_4) and radio-carbon (^{14}C) were ruled out due to the overall costs associated with purchasing the tracer mixture and/or the subsequent analysis. Other tracers such as many of the perfluorocarbons that have been used for in-reservoir monitoring were ruled out because they would be liquid at in-situ conditions (13 bar absolute pressure).

A customised gas storage system was built accommodating 3.3 t of liquid CO_2 with ~1.7 m^3 of CO_2 vapour headspace. The presence of two-phase CO_2 in the CO_2 tanks meant that the tracers could not be simply

added to the storage tanks but had to be mixed into the CO_2 gas flow to ensure constant tracer concentration.

The concentrated mixture of the trace gases (0.11 % C_3F_8, 1.77 % SF_6, 58.98 % Kr in a balance of CO_2 gas; BOC, UK) was stored in 4 x 50 L bladder accumulators (QHP, UK; bladder material: Viton) at 30 bar filling pressure positioned on the gas rig (Fig. 1). The accumulators were kept charged to a constant pressure of 30 bar via a regulated gas feed from the bulk CO_2 tanks. This was necessary to aid stability of flow and to ensure that nearly all of the mixture could be extracted when submerged at 120 m water depth with an external pressure of approximately 12 bar. The trace gas mixture was fed into a bespoke control unit where the flow was regulated through a mass flow controller (MFC) (Bronkhorst, UK) and then mixed into the main CO_2 line. The mixed gas line then re-entered the control unit where a second MFC regulated the overall flow rate. The gas mixture was delivered into the sediment at ~0.7 bar above ambient pressure. The MFCs worked as a master-slave pair whereby the mixed gas flow was user-controlled and the trace gas mix flow maintained a pre-set mass ratio. For the experiment the CO_2: tracer ratio was set at 10,000:1 to yield mole fractions of 58.98 ppm Kr, 1.77 ppm SF_6 and 0.11 ppm C_3F_8 in the final injection gas. This CO_2: tracer ratio was selected on the basis of (i) using the minimum amount of tracer while (ii) taking into account analytical detection limits of the tracers in the gas phase and in the water phase (ppb-ppt levels). The target CO_2:tracer injection ratio was kept constant throughout the release experiment.

The expected aqueous solubilities of tracers at in-situ conditions were calculated using the 'discrete bubble model' of the texas A&M oilspill calculator (TAMOC) model (Socolofsky, 2015; Gros et al., 2016; Gros et al., 2017; Dissanayake et al., 2018). The TAMOC model calculates the aqueous solubilities of gas mixtures based on fugacities calculated using the Peng-Robinson equation of state and the pressure-, temperature-, and salinity-dependent Henry's law constant (Gros et al., 2016). The model was tailored to each of the tracers based on ten chemical properties (Gros et al., 2021). The TAMOC model has been validated with field and laboratory data for a variety of pure gas and gas mixtures as well as for liquid petroleum hydrocarbons at conditions encompassing 1–150 bar (Dissanayake et al., 2018; Gros et al., 2016, 2017, 2019, 2021; Jun, 2018; Leonte et al., 2018).

2.3. Gas sampling

Gas was sampled using custom-made gas bubble samplers (GBS) (Corsyde, Germany) that were operated by the manipulator arms of the remotely operated vehicle (ROV) *Isis*. The GBS consisted of an inverted transparent funnel (0.7 L internal volume), inlet valve, stainless steel sample cylinder (0.5 L internal volume) and outlet valve (Fig. 2). Prior to sampling, the GBS were flushed with nitrogen (N_2) for several minutes and then evacuated to ~2×10^{-5} bar (Edwards High Vacuum Pump E2M5). Available space on the ROV was limited to 3 GBS that were attached to the lid of a box positioned on the sliding tray of the ROV (Fig. 2a). Gas samples were usually taken once a day and usually several hours after the gas flow rate was changed to avoid picking up a spike signal. Gas was collected from (i) the CO_2 release system's sample point (from here on referred to as rig gas samples) (Fig. 2b, c), (ii) from bubble streams at ~0.10–0.15 m above sea floor (masf) (from here on referred as seep gas samples) (Fig. 2d) and (iii) occasionally from the same bubble stream but at ~0.9–2.7 masf. The rig gas samples were used to identify any temporal variability of the CO_2:tracer ratio in the injection gas so that changes in the composition of the bubble stream samples could be accurately computed. Gas samples from ~0.9–2.7 m above the seabed were collected to validate numerically-simulated rates of CO_2 dissolution in the water column (Gros et al., 2021) and are not further discussed here. Markings on the funnel helped to identify the volume of gas collected over a given time period, providing a quantification of the flow rate from the bubble stream.

2.3.1. Gas analysis

2.3.1.1. CO_2, C_3F_8, SF_6, CH_4. A flow-through Fourier-Transmission Infra-Red (FT-IR) analyser (*atmos*FIR, Protea Ltd. UK) (S1, Supplementary Material) was used on board the RRS *James Cook* to measure the molar fractions of CO_2, SF_6, C_3F_8 and CH_4 in the discrete gas samples collected during the release experiment. The FT-IR was equipped with a custom-made sample injection system allowing reference gases to be injected (S1, Supplementary Material). The standard deviation (SD) (±1σ) and relative standard deviations (RSD) reported here for the individual tracer gas concentrations refer to the standard deviation of 6–10 analyses of the same gas sample. The RSD of C_3F_8 measurements
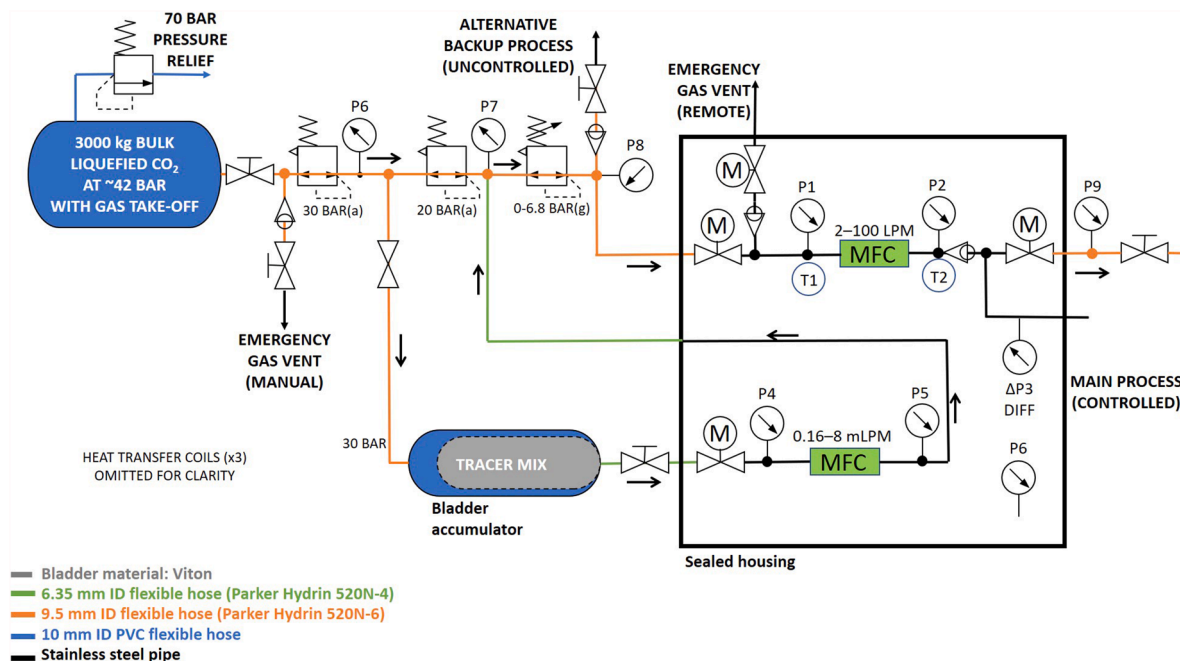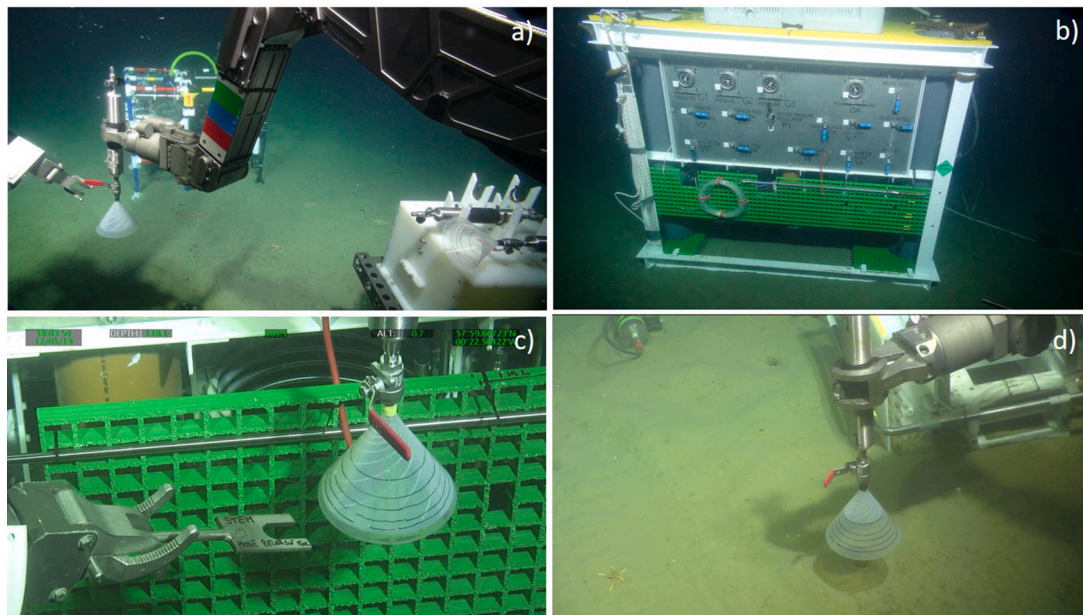

Fig. 1. Schematic overview of the gas flow path. Materials used are indicated by the colour coding.

Fig. 2. Gas sampling. (a) The GBS were operated by the ROV manipulator arms and stored on the sliding tray of the ROV. (b) Front panel of the gas rig and (c) gas sampling at the sample point (red tube) of the gas rig. (d) Gas sampling of a bubble stream close to the seabed at the experimental site. (For interpretation of the references to colour in this figure legend, the reader is referred to the web version of this article.)

Table 1
CO_2 injection flow rates. Note: accumulated tracer mass is calculated from the targeted tracer injection.

Start (date time UTC)	End (date time UTC)	CO_2 injection rate			
		L min^{-1}	g min^{-1}	kg d^{-1}	mol d^{-1}
11 May 2019 15:19	14 May 2019 15:27	2	4	6	128
14 May 2019 15:27	15 May 2019 06:48	5	10	14	291
15 May 2019 06:48	17 May 2019 16:54	10	20	29	645
17 May 2019 16:54	19 May 2019 15:50	30	59	86	1940
19 May 2019 15:50	22 May 2019 11:17	50	99	143	3234
				Total kg	**Total mol**
		CO_2 accumulated		675	14,780
		Tracers accumulated		0.08	

ranged from 0.4 to 18.7 %, for SF_6 from 0.1 to 2.0 % and for CH_4 from 0.2 to 1.4 % ($n = 26$). High RSDs of C_3F_8 and SF_6 were related to concentrations lower than optimal for the FT-IR.

The sampling port on the FT-IR instrument (S1, Supplementary Material) also allowed discrete sub-samples of the gas to be collected for later analysis of $\delta^{13}C_{CO2}$, $\delta^{18}O_{CO2}$ and Kr back onshore. Discrete gas samples were retrieved from the sampling port using gas tight syringes (Hamilton; needle diameter 0.3 mm). For each discrete sample, 25 mL of gas (at ambient temperature and pressure) was retrieved and injected into pre-evacuated 12 mL Exetainers® with double wadded septa (Labco). The gas samples were stored at room temperature.

2.3.1.2. $\delta^{13}C_{CO2}$, $\delta^{18}O_{CO2}$. The isotopic compositions of the discrete gas samples ($\delta^{13}C_{CO2}$, $\delta^{18}O_{CO2}$) were determined after the release experiment using a Delta V Advantage isotope mass spectrometer fitted with a GasBench II at the Department of Earth Sciences, University of Oxford. The samples were calibrated with NBS-18 and NBS-19 calcite standards,

at 50 °C. An acid fractionation factor $\alpha_{CO2(acid)-calcite} = 1.00934$ was applied to account for the difference in acid fractionation factor between the calcite standards and the gas samples (Kim et al., 2015). The relative $^{13}C/^{12}C$ values are reported in the conventional $\delta^{13}C$ (‰) notation, relative to the Vienna Pee Dee Belemnite (V-PDB), by assigning a value of $+1.95$ ‰ to NBS-19. The relative $^{18}O/^{16}O$ values are reported in the conventional $\delta^{18}O$ (‰) notation, relative to Vienna Standard Mean Ocean Water (V-SMOW), on a scale normalised such that the $\delta^{18}O$ of SLAP2 water was -55.5 ‰. Analytical accuracy ($\pm 1\sigma$) determined by measuring standards was ± 0.014 ‰ for $\delta^{13}C_{CO2}$ and ± 0.14 ‰ for $\delta^{18}O_{CO2}$, while analytical reproducibility ($\pm 1\sigma$) was ± 0.03 ‰ ($n = 7$) for $\delta^{13}C_{CO2}$ and ± 0.05 ‰ ($n = 7$) for $\delta^{18}O_{CO2}$.

2.3.1.3. Kr. The Kr concentration in the discrete gas samples was measured after the cruise using a portable quadrupole mass spectrometer (MiniRUEDI) (Brennwald et al., 2016) at the Department of Earth Sciences, Oxford. For quantitative analysis of Kr concentrations in CO_2, a specific measurement protocol had to be developed (S2, Supplementary Material). Calibration reference gases were created by mixing pure industrial grade CO_2 gas (BOC) with Kr-rich certified references gases. A total of 25 mL of gas was injected to ensure that the Exetainers® were over-pressured by the same amount as the samples. Five sets of reference gases were created, providing Kr concentrations of 45 ppm, 90 ppm, 261 ppm, 504 ppm, and 1506 ppm. This suite of reference gases was characterised using the MiniRUEDI and the data were used to create a calibration curve correlating measured intensity at m/z 84 with the known concentration of total Kr in the reference gases.

Each sample Exetainer® was analysed in two stages. First, an initial characterisation stage identified the gas species present and was used to make a rough assessment of the likely Kr concentration based on the calibration curves, and to allow the most appropriate calibration reference gas to be selected. Next, signal intensities at $m/z = 84$ were measured using both Faraday (less sensitive) and Secondary Electron Multiplier (more sensitive) detectors. Finally, a calibration reference gas of appropriate concentration was measured immediately after the sample, and using exactly the same measurement procedure as for the sample. Relative analytical uncertainties on signal intensities were typically 0.7–1.5 %.

Calculation of Kr concentrations from spectrometer intensities was

achieved by comparing blank-corrected intensities of the sample to blank-corrected intensities of the calibration reference gas and converting to concentrations via Eq (1):

$$\left[^{84}Kr\right] = \frac{Sample_{measured}}{Reference_{measured} / Reference_{true}} \qquad (1)$$

The concentration of elemental Kr was then calculated from the concentration of ^{84}Kr by assuming that the isotopic composition of the pure Kr gas is the same as atmospheric Kr (i.e., ^{84}Kr is 57 % of the total Kr concentration (Ozima and Podosek, 2002)). The assumption that Kr was unfractionated in sample gases was confirmed for the injected Kr by comparing signal intensities at $m/z = 84$ and $m/z = 86$ from analyses of air and the reference gases. Quoted standard deviations on Kr concentrations (RSD ranges from 1.2 to 4.9 %) include uncertainties associated with small differences in filling pressure between Exetainers®.

As Kr analyses took place ~3 months after the gas was sampled, sample quality and containment had to be verified. Measurements of the N_2/CO_2 ratios in the gas samples were used as a measure of sample containment over time assuming that atmospheric contamination of the gas sample would be reflected in a gradual increase of the N_2/CO_2 ratio. The N_2/CO_2 ratio in primary standards measured 1–4 days after filling (0.069 ± 0.0045, RSD $= 6.6$ %, $n = 5$) was virtually identical to those measured after 56 days (0.069 ± 0.0037, RSD $= 5.6$ %, $n = 3$) indicating that contamination by air during sample storage was negligible.

2.3.2. Quantification of CO₂ loss from the injected gas using the tracers

The tracer approach is based on the strong difference in trace gas solubility versus CO_2 solubility in seawater. Consequently, as the injected CO_2 migrated through the sediment, CO_2 dissolution into the sediment pore water was assumed to be the dominant process modifying the gas composition over time, with preferential loss of CO_2 from the gas phase leading to a gradual increase in tracer concentrations relative to CO_2 concentration in the remaining gas. The change in the tracer gas composition (Δc_{tracer}) between the initial rig gas sample (c_{tracer}^{rig}) and seep gas sample (c_{tracer}^{seep}) was derived as follows:

$$\Delta c_{tracer} = \left(\left(c_{tracer}^{rig} - c_{tracer}^{seep} \right) / c_{tracer}^{seep} \right) \times 100 \qquad (2)$$

and is equivalent to the percentage of CO_2 lost from the initially injected CO_2 due to dissolution in sediment pore water. For quantification, these values were referenced to the respective injected flow rate. It was further assumed that the composition of injected CO_2 measured in a seep gas sample was the same for all the seeps/bubble streams observed emanating from the seabed at that time. This simplification was necessary because time and space constraints meant that only one bubble stream could be sampled on any one ROV dive.

Depending on the intensity of the sampled bubble stream, sampling took between 23 min at lowest injection flow rates and 3 min at the highest injection flow rate. Consequently, the longer the sampling took, the longer the CO_2 within the funnel was in contact with water and thus continued to dissolve. To estimate the extent of dissolution within the inverted funnel during sampling, a typical mass transfer equation for a flat interface following the stagnant film model was applied (White et al., 2006):

$$F = (D / \delta) * \left(C_{eq} - C_{amb} \right) \qquad (3)$$

where F is the mass flux across the gas-water interface within the funnel (kg m^2 s^{-1}); D is the diffusion coefficient of CO_2 in seawater (m^2 s^{-1}); δ is the thickness of the boundary layer (m); C_{eq} is the concentration in seawater at equilibrium with the gas at in-situ conditions of pressure, temperature, and salinity (kg m^{-3}); and C_{amb} is the background concentration in ambient water (kg m^{-3}); $D = 9.9$ x 10^{-10} m^2 s^{-1}; $\delta = 165$ x 10^{-6} (m) (White et al., 2006); $C_{eq} = 24.1$ kg m^{-3}; and $C_{amb} << C_{eq}$ (based on field data) were assumed, such that ($C_{eq} - C_{amb}$) $\approx C_{eq}$. Equation 3 was integrated to estimate the total mass of CO_2 lost from the inverted funnel during sampling (m_{tot}, determined where $m_{tot} = \int_{0}^{total\ sampling\ time} A(t) \cdot F\ dt$, and $A(t)$ is the time-dependent surface area of the gas-water interface within the inverted funnel).

2.3.3. Direct measurement of gas bubble leakage flow rate

The gas bubble leakage rate across the seabed was estimated by measuring the time taken to fill the inverted funnel in 100 mL steps shown by the markings on the funnel. In most cases, 5 individual measurements were made for each bubble stream, but sub-optimal camera perspective/angle or funnel tilting meant that not all measurements were reliable.

Seeps varied in intensity and thus leakage rate during each sampling campaign. Although a number of bubble streams were active at any one time (as recorded by ROV video footage), leakage rate measurements could only be made from one bubble stream (usually one of the most constant and intense ones) per ROV dive. Flow rates for other bubble streams were estimated by re-viewing the ROV video footage, visually comparing bubble streams to the sampled bubble stream, and determining their relative intensities (either 25, 50, 75, 100 % relative to the sampled bubble stream). The total leakage rate was defined as the number of bubble streams multiplied by their assigned leakage rate.

The difference between the total estimated bubble leakage rate and total injected CO_2 was assumed to represent CO_2 that remained in the sediment. This CO_2 may consist of both dissolved and gaseous CO_2. As tracers only quantify CO_2 in the dissolved phase, the difference between these two values was used to approximate the fraction of gaseous CO_2 that remained in the sediment.

2.4. Seawater and pore water samples

2.4.1. Sampling

Seawater samples were taken using Niskin bottles (1.7 L) mounted at the back of the ROV. Usually 4 Niskin bottles were fired above the bubble stream between 1.5–2.5 m above the seafloor, and 2 Niskin bottles were fired close to the gas rig, both towards the end of the dive. The sampling was done by reversing the ROV above the bubble stream, using the rear camera that was aligned with the Niskin bottles, and firing the bottles when gas bubbles were visible between or close to the Niskin bottles. After recovery, water samples were retrieved from the Niskin bottles. Water samples for analyses of dissolved inorganic carbon (DIC), and carbon and oxygen isotopes ($\delta^{13}C_{DIC}$, $\delta^{18}O_{H2O}$) were collected following standard operation procedures (Dickson et al., 2007), were filled in 12 mL Exetainer® borosilicate glass vials (Labco) and 40 mL borosilicate glass vials (Thermo) with no headspace, poisoned with $HgCl_2$ and stored upside down at room temperature.

Sediment cores for retrieval of pore water samples were collected during cruise JC180. A detailed description of the sampling and processing of the sediment cores is given elsewhere (Lichtschlag et al., 2021). Up to six 30 cm long x 8 cm diameter push cores were taken with the ROV on selected dives at each injection rate as well as before and after the CO_2 was injected. Coring locations were selected whilst watching the live camera feed from the ROV, such that cores were taken as close as possible to seabed bubble streams. Background cores were taken at least 25 m away from the bubble streams. After recovery, the push cores were processed in a controlled temperature lab set to the in-situ water temperature (7 °C), the overlying water was removed and the cores were transferred to a N_2-filled glove box to minimise oxidation of redox-reactive compounds. The cores were sliced in 1 cm depth intervals for the top 10 cm and in 2 cm intervals at depths greater than 10 cm below the seafloor. The sediment slices were transferred to 50 mL centrifuge tubes for pore water extraction using Rhizon Soil Moisture samplers (Rhizon CSS: length 5 cm, pore diameter 0.2 μm; Rhizosphere Research Products, Wageningen, Netherlands). The pore waters were

sub-sampled for analysis of DIC, $\delta^{13}C_{DIC}$ and $\delta^{18}O_{H2O}$. Since the sediment cores and the N_2-chamber where not pressure-compensated, the DIC and $\delta^{13}C_{DIC}$ in pore water were affected by degassing during core retrieval and core processing.

2.4.2. Analysis

The DIC content of water column samples was measured using an Apollo AS-C3 DIC Analyser at the National Oceanography Centre, Southampton. The relative precision was <0.1 %, and the accuracy of undiluted samples was ± 4 μmol kg^{-1}. The pore water samples were diluted with MilliQ by a factor of 5 and were measured on an Apollo (AS-D1) DIC analyser coupled to a Picarro G-2131i analyser. The analytical precision of diluted samples was <0.5 % and the accuracy was ± 15 μmol kg^{-1}. In both cases analyses were calibrated against certified reference material for oceanic CO_2 measurements supplied by A. Dickson (University of California, Scripps Institution of Oceanography, San Diego, USA).

The isotopic compositions of the water samples ($\delta^{13}C_{DIC}$, $\delta^{18}O_{H2O}$) was measured using a Delta V Advantage isotope ratio mass spectrometer fitted with a GasBench II at the Department of Earth Science, University of Oxford (Section 2.3.1.2), based on methods described in Assayag et al. (2006) for $\delta^{13}C_{DIC}$, and Nelson (2000) for $\delta^{18}O_{H2O}$.

3. Results

3.1. Bubble streams

After CO_2 injection was started, bubbles were observed emerging from the seabed as soon as the ROV reached the injection site, i.e., within ~30 min. Over the duration of the release experiment the number of active bubble streams ranged from 3 at the lowest injection rate (6 kg d^{-1}) to a maximum of 15 at an injection flow rate of 86 kg d^{-1} (Table 2). All of the observed bubble streams were located within a ~4 m radius of the CO_2 injection point within the sediments, and most were clustered ~2 m to the south of this point.

Overall, the locations of the bubble streams were quite variable, i.e., within a day seeps would disappear, branch out and re-appear a few centimetres away from the initial seep location. Consequently, although there were 12 active bubble streams observed on the last day of the experiment (D+10, 143 kg d^{-1}), an additional 14 inactive pockmarks were visible on the sediment surface marking the position of previously active bubble streams. Bubble stream intensity was also variable, i.e., bubble flow changed from constant to intermittent and from strong to weak. The intermittent bubble streams were quite continuous for a while and then disappeared to re-appear after a short time later, which indicates that gas was pooling in the sediment until a certain overpressure

Table 2

Direct measurements of CO_2 seepage rate across the seabed in the gas phase relative to the CO_2 injection rate at 3-m depth into the sediment. The volume injection rate refers to the volume at in-situ conditions assuming an average water depth of 120 m, a salinity of 35 (absolute pressure of 13.1384 bars), and a temperature of 7.7 °C.

ROV dive #	Date	Day	Injection rate			ID	In-situ measured leakage rate from a single seep	Total # of seeps	Total # of equiv. seeps	In-situ total leakage rate across seabed	Total leakage across seabed	Total leakage across seabed
			kg d^{-1}	mol d^{-1}	L min^{-1}, in-situ		L min^{-1}			L min^{-1}	% of injected CO_2	kg d^{-1}
358	12/05/2019	D+1	6	128	0.152	1	0.014±0.002	4	3	0.043±0.006	28.4±3.8	1.7±0.2
359	12/05/2019	D+1	6	128	0.152	2	0.028±0.005	4	1.75	0.049±0.009	32.4±5.6	1.9±0.3
360	13/05/2019	D+2	6	128	0.152	3	0.011±0.002	5	3	0.033±0.007	21.6±4.5	1.3±0.3
361	13/05/2019	D+2	6	128	0.152	4	0.018±0.002	3	2	0.036±0.004	23.5±2.4	1.4±0.1
363	15/05/2019	D+4	29	645	0.761	5	0.050±0.018	6	4.25	0.211±0.077	27.7±10.1	8.0±2.9
366	16/05/2019	D+5	29	645	0.761	6	0.079±0.010	8	3.3	0.261±0.032	34.2±4.1	9.9±1.2
369	17/05/2019	D+6	29	645	0.761	7	0.052±0.006	5	3.3	0.170±0.021	22.4±2.8	6.5±0.8
370–1	18/05/2019	D+7	86	1940	2.283	8–1	0.200±0.020	8	6.5	1.300±0.130	56.9±5.7	49.0±4.9
370–2	18/05/2019	D+7	86	1940	2.283	8–2	0.203±0.019	8	6.5	1.317±0.125	57.7±5.5	49.6±4.7
372	19/05/2019	D+8	86	1940	2.283	9	0.080±0.008	13	6.9	0.552±0.057	24.2±2.5	20.8±2.1
373	19/05/2019	D+8	86	1940	2.283	10*	0.324±0.012	15	5	1.622±0.062	71.0±2.7	61.1±2.3
375	20/05/2019	D+9	143	3232	3.806	10*	0.522±0.077	12	3.5	1.826±0.270	48.0±7.1	68.6±10.1
376	21/05/2019	D+10	143	3232	3.806	10*	0.364±0.115	12	4.0	1.455±0.458	38.2±12.0	54.7±17.2

*same seep sampled on consecutive days.

was reached, which then initiated bubble release until the overpressure was compensated.

After the CO_2 injection was stopped, the ROV returned to the experimental site ~3 hrs later. By then all of the bubble streams had disappeared. There was no evidence for bubble emission from the sediments during infrastructure recovery, during any of the post-injection sampling (e.g., sediment coring), and during the final AUV and ROV surveys, which took place up to 3 days after the CO_2 injection was stopped.

3.2. Gas samples

3.2.1. Composition and isotopic signature of injected CO_2

The target CO_2:tracer ratio was kept constant at 10,000:1 and the injection flow rate was gradually increased from 6 kg d^{-1} to 143 kg d^{-1} during the experiment (Table 1). Analyses of the rig gas samples indicated that the tracer concentrations in the CO_2 fluctuated significantly especially at low injection flow rates (6 and 29 kg d^{-1}). Measured tracer concentrations were between ~20 to 6000 % of their expected concentration consistent with the range observed during onboard tests (S3, Supplementary Material). However, at higher injection flow rates (86 and 143 kg d^{-1}) tracer concentrations were closer to the expected values, ranging from 44 to 103 % of their expected concentration. Crucially, ratios of SF_6:C_3F_8, Kr:SF_6 and Kr:C_3F_8 stabilised close to their expected values, which provided confidence in the robustness of tracer injection at these higher flow rates. CH_4 was initially present in trace quantities of ~54 ppm in the vapour headspace of the main CO_2 tanks. Over the duration of the experiment CH_4 concentrations within the vapour headspace gradually decreased to ~33 ppm. This decrease is tentatively attributed to preferential partitioning of CH_4 to the vapour headspace with respect to the liquid within the CO_2 tanks, leading to preferential depletion of CH_4 with respect to CO_2 during withdrawal of gas from the vapour headspace over the course of the experiment. This interpretation is supported by a larger fugacity coefficient for CH_4 than for CO_2 within the liquid CO_2 (calculated using the Peng-Robinson equation of state as implemented in TAMOC). As CH_4 was pre-mixed with the CO_2 in the CO_2 tanks, the CO_2:CH_4 ratio was nevertheless more constant than the CO_2:tracer ratio, especially at low flow rates, meaning it could be utilised as a reference gas against which tracer gas data could be compared. Given the variability of C_3F_8, SF_6 and Kr concentrations at low (6 and 29 kg d^{-1}) injection rates, the quantification estimates for these flow rates are based on CH_4 only.

The CO_2 in the main tank and in the tracer mixture were purchased from different vendors and had different isotopic $\delta^{13}C_{CO2}$ signatures. On average, the CO_2 of the main tank showed an isotopic signature of $\delta^{13}C_{CO2} = 18.554 \pm 0.056$ ‰ and $\delta^{18}O_{CO2} = 32.493 \pm 0.031$ ‰ (n = 5). The CO_2 of the tracer mixture had an isotopic signature of $\delta^{13}C_{CO2} = 5.193 \pm 0.032$ ‰ and $\delta^{18}O_{CO2} = 28.208 \pm 0.052$ ‰ (n = 6). The above gas

samples were collected on land, i.e., these gas samples had not been in contact with seawater. In contrast, the gas samples of the CO_2 mixture were collected during the release experiment via the funnel technique, i.e., the rig gas sample had been in contact with seawater during the sampling procedure. After mixing, the CO_2 mixture had an isotopic signature of $\delta^{13}C_{CO2} = 19.036 \pm 0.054$ ‰ and $\delta^{18}O_{CO2} = 33.730 \pm 0.464$ ‰ (n = 11). Both values are higher than expected from a 10,000:1 CO_2:tracer mix caused by isotope fractionation effects (Vogel et al., 1970; Bottinga, 1968) (see also S6, Supplementary Material).

The presence of inherent CH_4 in the main CO_2 tank and the high $\delta^{13}C_{CO2}$ value of this CO_2 (AirLiquide, UK) reflects the origin of the CO_2; the CO_2 was generated by anaerobic digestion of biomass crops and this process produces CO_2 with heavy $\delta^{13}C_{CO2}$ values as well as CH_4 (Lv et al., 2019). The CO_2 is then distilled to EIGA (European Industrial Gases Association) food grade quality, which permits trace amounts (~50 ppm) of CH_4 (EIGA, 2016).

3.2.2. Composition and isotopic signature of gas from bubble streams

As mentioned above, tracer injection into the main CO_2 supply was instable at low injection flow rates (6 and 29 kg d^{-1}) occasionally causing C_3F_8, SF_6 and Kr tracer mole fractions in seep gas samples to be lower than in the corresponding rig gas sample (S4, Supplementary Material). Thus, for 6 and 29 kg d^{-1} injection rates, only CH_4 results will be discussed in detail.

At the $\geq$86 kg d^{-1} injection levels, all tracer mole fractions in the seep gas samples were higher than in the corresponding rig gas sample suggesting that transient spikes in the tracer/CO_2 ratio were insignificant. Replicate gas samples taken from the same seep shortly after one another (ROV#370, 86 kg d^{-1}) varied by $\pm$7.6 % for C_3F_8, $\pm$7.2 % for SF_6, $\pm$9.8 % for Kr and by $\pm$1.6 % for CH_4 (n = 2).

The $\delta^{13}C_{CO2}$ values of seep gas samples captured close to the seabed ranged from 19.45 to 20.25 ‰ (n = 8) and from and 20.55 to 21.66 ‰ (n = 3) when collected at ~0.9–2.7 m masf (S4, Supplementary Material). The change in $\delta^{13}C_{CO2}$ of rig gas samples compared to seep gas samples was used to quantify CO_2 dissolution in the sediment pore water (S6, Supplementary Material) and in the water column (Gros et al., 2021).

The $\delta^{18}O_{CO2}$ values of seep gas samples captured close to the seabed ranged from 34.652 to 39.590 ‰ (n = 8) and from 34.920 to 35.209 ‰ (n = 3) when collected at ~0.9–2.7 m masf (S4, Supplementary Material). In contrast to the $\delta^{18}O_{CO2}$ values of rig gas samples, the variability of $\delta^{18}O_{CO2}$ of rig gas samples was considerably higher and beyond the analytical uncertainty. A positive correlation between $\delta^{18}O_{CO2}$ and sample storage time, i.e., the time that passed between gas sampling and analysis (2.4 to 8.9 hrs) (not shown), is suggestive of a sampling artefact. This was likely caused by continuing oxygen isotope fractionation between CO_2 and (condensed) H_2O vapour in the gas bubble samplers. Due to this sampling artefact, the $\delta^{18}O_{CO2}$ values were not used for further simulations.
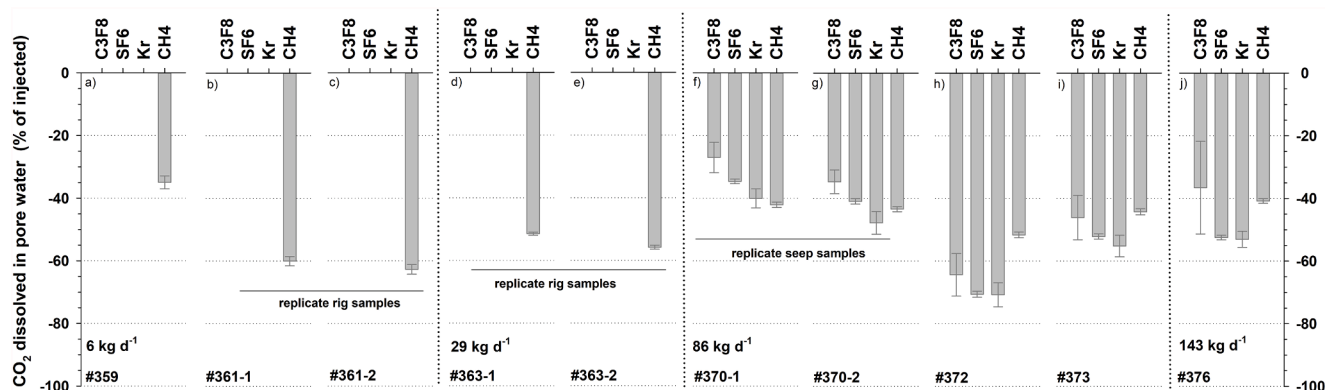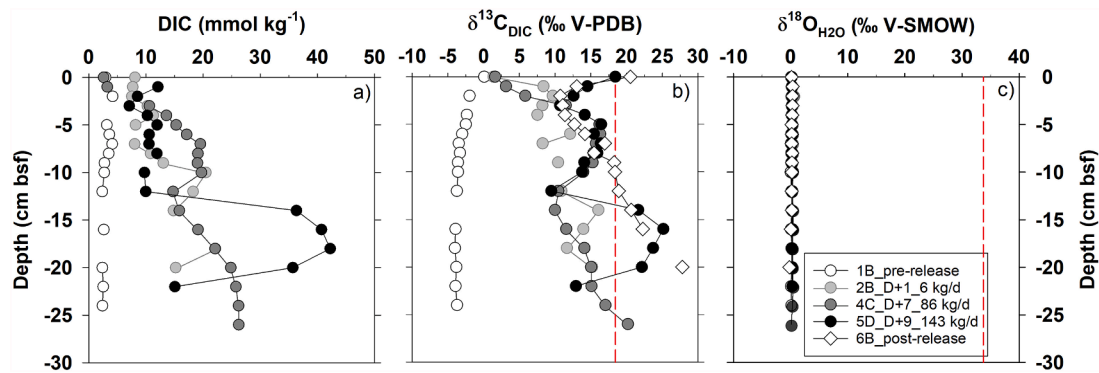

Fig. 3. Tracer-based estimates of CO_2 dissolution in sediment pore waters for all seeps sampled (see also S4, Supplementary Material).

Fig. 4. Pore water chemistry in selected cores sampled before, during and after the injection of the CO_2 into the sub-seabed sediments. (a) Vertical profile of DIC, b) $\delta^{13}C_{DIC}$ and c) $\delta^{18}O_{H2O}$ in pore water samples. The red dashed lines in (b) and (c) indicate the isotopic signature of injected CO_2. Please note: no DIC measurements are available for 6B_post-release. (For interpretation of the references to colour in this figure legend, the reader is referred to the web version of this article.)

3.2.3. Quantification of CO_2 dissolution in sediment pore waters

Tracer-based quantification of CO_2 loss to the dissolved phase during the 3-m vertical ascent through the sediments are given in Fig. 3 and Table 3.

At the lowest injection rate of 6 kg d^{-1}, CH$_4$-based estimates indicate that between 2.1±0.1 and 3.8±0.1 kg d^{-1} of the injected CO_2 (35–63 %) dissolved in sediment pore waters. Estimates from replicate rig samples agreed within ±1.5 % (ROV#361).

At 29 kg d^{-1} injection rate, CH$_4$-based estimates from replicate rig samples (ROV#363) suggest that 16±1 kg d^{-1} (52-56 % of the injected CO_2) dissolved in sediment pore waters.

At 86 kg d^{-1} injection rate, CH$_4$-based estimates suggest that 36±1 to 44±1 kg d^{-1} (42–52 % of the injected CO_2) dissolved in sediment pore waters. Estimates based on analyses of added tracers were similar, ranging from 23±4 to 55±6 kg d^{-1} for C_3F_8, from 29±1 to 61±1 kg d^{-1} for SF_6 and from 34±3 to 61±3 kg d^{-1} for Kr. Replicate samples collected from the same bubble stream (ROV#370_1, 370_2) agreed within ±1 % for CH$_4$, ±4.8 % for C_3F_8, ±4.5 % for SF_6 and ±5.6 % for Kr.

At the highest injection rate of 143 kg d^{-1} the CH$_4$-based estimate suggested that 58±1 kg d^{-1} (41 %) of the injected CO_2 dissolved in sediment pore waters. Added tracer-based estimates were 52±21 kg d^{-1} for C_3F_8, 75±1 kg d^{-1} for SF_6 and 76±4 kg d^{-1} for Kr.

Overall, the dissolution estimates of CH$_4$, C_3F_8, SF_6 and Kr are statistically not significantly different (ANOVA, $\alpha = 0.05$). On average, the amount of CO_2 dissolution estimates of added tracers deviated by −3 to 10 % ($n = 5$) from CH$_4$-based estimates. Residuals from the CH$_4$-based estimates ranged from −15 to +13 % ($\bar{x} = -3\pm11$ %, $\tilde{x} = 4$ %, $n = 5$) for C_3F_8, −7 to +18 % ($\bar{x} = 6\pm11$ %, $\tilde{x} = 8$ %, $n = 5$) for SF_6 and −2 to +20 % ($\bar{x} = 9\pm8$ %, $\tilde{x} = 9$ %, $n = 5$) for Kr. The coefficient of variance (the ratio of the standard deviation to the mean) was −4 % for C_3F_8, 2 % for SF_6 and 1 % for Kr and shows that the relative variability of the residuals was largest for C_3F_8 and lowest for Kr. The larger variation of C_3F_8 residuals can be explained by the overall analytical uncertainty. High RSD values of >5–12 % were associated with very low C_3F_8 concentrations (<0.1 ppmv) in the sample gas suggesting C_3F_8 concentrations of <0.1 ppmv were below the optimal detection range of the analyser. Only the CH$_4$-based estimates of CO_2 dissolution in sediment pore waters are discussed herein since they cover all injection flow rates tested.

CO_2 loss during sampling (which took between 3 and 23 min) due to dissolution of the gas within the inverted funnel was estimated to be 1.5–11 %, which was considered to be insignificant. The dissolution of tracers in pore water affected the calculated percentages of CO_2 dissolution in the sediment by ≤0.3 % of the injected CO_2 for C_3F_8 and SF_6, ≤2.7 % for Kr and ≤0.97 % for CH$_4$, based on mass transfer calculations

Table 3

Estimates of CO_2 dissolution in sediment pore waters based on tracers. Estimates are derived by comparing the increase in tracer concentration relative to CO_2 measured between the injected CO_2 and the CO_2 issuing from seabed bubble seeps, assuming negligible tracer dissolution.

ROV dive #	Date	Day	Injection rate			ID	C_3F_8	SF_6	Kr	CH$_4$	C_3F_8	SF_6	Kr	CH$_4$
			kg d^{-1}	mol d^{-1}	L min^{-1}		Loss of CO_2 from CO_{2mix} (%)				Loss of CO_2 from CO_{2mix} (kg d^{-1})			
359	12/05/2019	D+1	6	128	2	2	–	–	–	−35.0 ±2.1	–	–	–	−2.1 ±0.1
361–2	13/05/2019	D+2	6	128	2	4–1	–	–	–	−60.0 ±1.5	–	–	–	−3.6 ±0.1
361–1	13/05/2019	D+2	6	128	2	4–2	–	–	–	−63.0 ±1.5	–	–	–	−3.8 ±0.1
363–1	15/05/2019	D+4	29	645	10	5–1	–	–	–	−51.5 ±0.5	–	–	–	−14.9 ±0.1
363–2	15/05/2019	D+4	29	645	10	5–2	–	–	–	−55.8 ±0.6	–	–	–	−16.2 ±0.2
370–1	18/05/2019	D+7	86	1940	30	8–1	−27.9 ±4.8	−34.6 ±0.8	−40.0 ±3.0	−42.1 ±0.8	−23.2 ±4.2	−29.8 ±0.6	−34.4 ±2.6	−36.2 ±0.7
370–2	18/05/2019	D+7	86	1940	30	8–2	−34.7 ±3.8	−41.0 ±0.8	−47.9 ±3.6	−43.4 ±0.8	−29.8 ±3.3	−35.2 ±0.7	−41.1 ±3.1	−37.3 ±0.7
372	19/05/2019	D+8	86	1940	30	9	−64.3 ±6.8	−70.6 ±0.9	−70.8 ±3.8	−51.6 ±0.9	−55.3 ±5.9	−60.7 ±0.8	−60.8 ±3.3	−44.4 ±0.8
373	19/05/2019	D+8	86	1940	30	10*	−46.1 ±7.1	−52.1 ±0.8	−55.2 ±3.5	−44.3 ±1.0	−39.6 ±6.1	−44.8 ±0.7	−47.4 ±3.0	−38.1 ±0.8
376	21/05/2019	D+10	143	3232	50	10*	−36.6 ±14.8	−52.5 ±0.8	−53.0 ±2.6	−40.8 ±0.8	−52.3 ±21.2	−75.0 ±1.1	−75.8 ±3.7	−58.3 ±1.1

*same seep sampled on consecutive days.

(Gros et al., 2021). These calculations assume that background pore waters contain 0.000536 mM CH_4 at 0–3 m depth (Linke and Haeckel, 2018), and background concentrations of Kr, SF_6, and C_3F_8 were assumed to be negligible. The calculated values for tracer dissolution into sediment pore waters are close to or lower than the analytical error and the variability determined from replicate measurements. The reported quantifications were thus corrected neither for tracer aqueous dissolution into sediment pore waters nor for dissolution from the inverted funnel during sampling.

3.2.4. Direct measurements of leakage rates from bubble streams

Bubble leakage rates derived from the volume of gas collected over a given time period are given in Table 2. A total of 13 measurements were made over the course of the experiment with in-situ leakage rates from a single bubble stream ranging from 0.011 ± 0.002 L min^{-1} at the lowest injection flow rate to 0.522 ± 0.077 L min^{-1} at the highest injection rate (Table 2). Overall, the incremental increase of the injection flow rate resulted in an increase of the total leakage rate from a minimum of 1.3 kg CO_2 d^{-1} at the lowest injection rate (6 kg d^{-1}) to a maximum of 68.6 kg CO_2 d^{-1} at the highest injection rate (143 kg d^{-1}). This gas leakage was distributed over a varying number of active bubble streams of different intensities, with the number of equivalent bubble streams ranging from 1.75 to 7 (Table 2).

Overall, the RSD of the 5 (or fewer) leakage rate measurements ranged from 0.2 to 36 % (median 12.1 %, $n = 13$). High RSD values were caused by changes in leakage rate intensity during sampling (observed at low injection levels), suboptimal camera perspective and/or funnel position (tilted), which hampered the visual estimation of gas volume.

3.3. Pore waters

Prior to the start of the CO_2 injection, the DIC concentration of the sediment pore waters ranged from 2.3 to 4.0 mmol kg^{-1} ($n = 10$). The background $\delta^{13}C_{DIC}$ varied between -1.9 and -4.0 ‰ (Fig. 4). Over the course of the experiment, the DIC content of the pore waters gradually increased, reaching concentrations of ~40 mmol kg^{-1}. Dissolution of released CO_2 ($\delta^{13}C_{CO2} = 19.4\pm0.92$ ‰) into the pore water caused a simultaneous increase in pore water $\delta^{13}C_{DIC}$ (Fig. 4) with $\delta^{13}C_{DIC}$ values of 19–27 ‰ observed in cores from $D+7$ onwards. No indication of dissolution of injected CO_2 ($\delta^{18}O_{CO2} = 32.5\pm0.03$ ‰, $n = 5$) was observed in the $\delta^{18}O_{H2O}$ signature of pore waters ($\delta^{18}O_{H2O} = 0.27\pm0.13$ ‰, $n = 80$) compared to background values ($\delta^{18}O_{H2O} = 0.20\pm0.11$ ‰, $n = 16$) (Fig. 4).

3.4. Water column

Concentrations of DIC in the bottom water sampled prior to the start of the CO_2 release experiment were on average 2154.6 ± 4.4 μmol kg^{-1} ($n = 7$). Throughout the CO_2 release experiment the average DIC concentration of bottom waters, sampled approximately 100 metres away from the release site, showed a similar average value of 2156.6 ± 3.0 μmol kg^{-1} ($n = 12$) (S5, Supplementary Material). The stable carbon isotopic signature of the DIC sampled away from the seabed bubble streams was $\delta^{13}C_{DIC} = 0.61\pm0.03$ ‰ ($n = 7$) prior to the release experiment and $\delta^{13}C_{DIC} = 0.60\pm0.06$ ‰ during and after injection of the CO_2 into the sub-seabed sediments. The oxygen isotopic signature of seawater was $\delta^{18}O_{H2O} = 0.30\pm0.1$ ‰ before the release of the CO_2 and $\delta^{18}O_{H2O} = 0.32\pm0.1$ ‰ ($n = 12$) during and afterwards.

Water samples taken between 2.5 and 3 metres above a seabed bubble seep were not enriched in DIC relative to background seawater when the CO_2 injection rate was 6 kg d^{-1}. As the injection rate was increased to 29 kg d^{-1}, the DIC content of bottom waters increased to 2176.6 ± 1.6 μmol kg^{-1} and there was a slight increase in $\delta^{13}C_{DIC}$ from ~0.61 ‰ to 0.69 ‰. During the 86 kg d^{-1} injection rate, DIC concentrations of up to 2725.3 ± 1.2 μmol kg^{-1} were observed along with significantly elevated $\delta^{13}C_{DIC}$ values of 5.22 ‰. At the highest injection

flow rate of 143 kg d^{-1}, the DIC and $\delta^{13}C_{DIC}$ concentrations were also elevated relative to background seawater but did not exceed 2321.9 ± 1.13 μmol kg^{-1} and 1.95 ‰, respectively. Overall, the DIC concentration showed a close correlation with $\delta^{13}C_{DIC}$ ($\delta^{13}C_{DIC} = 0.008\times DIC - 17.07$, $r^2 = 0.989$, $n = 42$) indicative of the impact of injected CO_2. No indication of dissolution of injected CO_2 was observed in the $\delta^{18}O_{H2O}$ signature of water column samples ($\delta^{18}O_{H2O} = 0.31\pm0.1$ ‰, $n = 42$) compared to background values.

4. Discussion

In this section, the applicability of natural, inherent tracers and added tracers for source attribution and detection (Section 4.1.) and for leakage rate quantification at the seafloor (Section 4.2) are discussed. The practicalities of tracer sampling and analysis are also discussed and finally recommendations for tracer use in marine environmental monitoring of offshore CO_2 storage sites are provided (Section 4.3).

4.1. Leakage detection and attribution during the STEMM-CCS release experiment

Regulations developed for CO_2 storage such as the IPCC guidelines (IPCC, 2006), the EU CCS Directive (EU, 2009), the London Protocol (IMO, 2006) and OSPAR (OSPAR, 2007) include mandatory monitoring of the storage complex. This includes the ability to detect a leakage (EU, 2009). Source attribution is not yet a legal requirement for CCS monitoring. However, from practical experience of monitoring of terrestrial CO_2 storage projects, thorough source attribution has proven to be essential to avoid false positives (Romanak et al., 2012; Romanak et al., 2014) and is likely to become an integral part of environmental monitoring protocols (Dixon and Romanak, 2015).

This study has shown that added tracers are capable of detecting and attributing leakage of the injected CO_2 in the marine system. C_3F_8, SF_6, Kr and CH_4 were detected in all gas samples taken from the bubble streams. The main natural source of dissolved C_3F_8, SF_6 and Kr in the marine environment is from the atmosphere via air-sea gas exchange at the ocean surface and subsequent mixing down to deeper water layers (Stanley and Jenkins, 2013; Tanhua et al., 2004), i.e., none of these gases has a significant biological or geochemical source in sediments of the North Sea. In contrast, so-called pockmark structures, which act as venting sites of CH_4 from deep thermogenic sources and shallow microbial methanogenesis, are potentially significant natural sources of CH_4 in sediments of the North Sea (e.g., Chand et al., 2017; Karstens and Berndt, 2015; Böttner et al., 2019; Judd et al., 1994). However, the CO_2 release experiment was performed away from active pockmarks, in a region where the main potential source of CH_4 in shallow sediments is from methanogenesis. In the wider Goldeneye area, methanogenesis only occurs at depths of >20 mbsf within the sediments (Dale et al., 2021) and is therefore not considered a source of CH_4 in sediments at <3 mbsf. Consequently, the detection of C_3F_8, SF_6, Kr and CH_4 in seep gas samples confirmed that the source of the leaked gas was the injected CO_2.

The increase of C_3F_8, SF_6, Kr and CH_4 mole fractions in seep gas samples compared to their initial mole fractions in the rig gas samples (S4, Supplementary Material) is indicative of the impact of preferential CO_2 dissolution into sediment pore waters and bottom water. Aqueous CO_2 dissolution was further confirmed by the increase of $\delta^{13}C$ signatures of rig gas samples ($\delta^{13}C_{CO2} = 19.04\pm0.1$ ‰) compared to seep gas samples collected directly above the seafloor ($\delta^{13}C_{CO2}$ up to 20.25 ‰) and at ~0.9–2.7 masf ($\delta^{13}C_{CO2}$ up to 21.66 ‰). Aqueous dissolution gradually enriched the remaining gaseous CO_2 with ^{13}C (Gros et al., 2021; Mayer et al., 2015; Zeebe and Wolf-Gladrow, 2001) (S5 and S6, Supplementary Material) caused by preferential dissolution of ^{12}C with respect to ^{13}C (Jähne et al., 1987; Vogel et al., 1970).

Geochemical analyses of the dissolved and solid phase of the sediments along with transport-reaction modelling suggest that the

dominant geochemical process in the sediments was CO_2 dissolution with only a minor contribution from carbonate dissolution (2 %) and silicate mineral dissolution (3 %) (Lichtschlag et al., 2021). CO_2 dissolution into sediment pore waters was confirmed by elevated DIC concentrations detectable at the lowest injection rate (6 kg d^{-11}). Overall, DIC values increased from a typical background of 2–3 mmol kg^{-1} to 40 mmol kg^{-1} at the highest CO_2 injection rate (143 kg d^{-1}) in sediment pore waters sampled close to the bubble streams. The increase in DIC was accompanied by a simultaneous increase in pore water $\delta^{13}C_{DIC}$ (up to 27 ‰) compared to background values ($\delta^{13}C_{DIC}$ = −2 to −4 ‰) (Fig. 4). Similarly, in the overlying water column, the presence of injected CO_2 was confirmed by elevated DIC concentrations but, unlike in the sediment pore waters, the bottom water CO_2 signal was quickly diluted, and the presence of injected CO_2 was only detectable at CO_2 injection rates of >29 kg d^{-1}. DIC concentrations increased to 2725 µmol kg^{-1} and were associated with a simultaneous increase of $\delta^{13}C_{DIC}$ to 5.22 ‰ compared to background values (DIC = 2155 µmol kg^{-1}, $\delta^{13}C_{DIC}$ = 0.61 ‰) (S5, Supplementary Material). The presence of injected CO_2 in bottom water was further confirmed by decreased in-situ pH (Schaap et al., 2021; Koopmans et al., submitted for publication).

Assuming the elevated $\delta^{13}C_{DIC}$ values of sediment pore waters and the bottom seawater were due to dissolution of all of the injected CO_2 then the highest expected $\delta^{13}C_{DIC}$ value would be ~19 ‰, which is lower than the highest $\delta^{13}C_{DIC}$ value measured (27 ‰). However, partial dissolution of injected CO_2 into sediment pore waters and its conversion to HCO_3^- and CO_3^{2-} fractionates carbon isotopes, enriching the HCO_3^- and CO_3^{2-} in ^{13}C relative to gaseous CO_2. The difference between $\delta^{13}C_{HCO3-}$ and $\delta^{13}C_{CO2}$ is approximately +10 ‰ at 7 °C, and the difference between $\delta^{13}C_{HCO3-}$ and $\delta^{13}C_{CO2}$ at the same temperature is approximately +6.9 ‰ (Zhang et al., 1995). Thus, $\delta^{13}C_{DIC}$ values of up to 29 ‰ are consistent with partial dissolution of the injected CO_2 and conversion to HCO_3^-, which is supported by the results of tracer analyses (Section 4.2; see also S6, Supplementary Material). Degassing of CO_2, e. g., during sample retrieval and sample processing, may also contribute to enrichment of ^{13}C in the DIC that remains in solution (Zeebe and Wolf-Gladrow, 2001). Overall, in line with findings from QICS (Lichtschlag et al., 2015), our results suggest that both $\delta^{13}C_{CO2}$ and $\delta^{13}C_{DIC}$ can be effective indicators of CO_2 leakage at least within the shallow sub-seafloor. Implementation of $\delta^{13}C$ tracing as an operational monitoring tool for leakage from a deep CO_2 storage reservoir may, however, be limited by more complex carbon isotope fractionation processes that can occur during migration through the overburden (Mayer et al., 2015), and also variations in the $\delta^{13}C_{CO2}$ source signature (Flude et al., 2016; Roberts et al., 2017). Studies based on simulations, lab experiments and empirical observations suggest that $\delta^{13}C$ can be a suitable indicator for CO_2 leakage detection from deep sub-seafloor CO_2 storage sites provided that the $\delta^{13}C$ value of injected CO_2 is isotopically distinct by >10 ‰ from the background $\delta^{13}C_{CO2}$ and $\delta^{13}C_{DIC}$ values (Shevalier et al., 2014; Rock et al., 2014; Mayer et al., 2015). In this study, the injected CO_2 was generated by anaerobic digestion of biomass crops that produces CO_2 with a high $\delta^{13}C_{CO2}$ signature ($\delta^{13}C_{CO2}$ = 19 ‰) (Lv et al., 2019), whereas the $\delta^{13}C_{CO2}$ value of CO_2 captured from industrial sources is much lower, usually between around −50 and −5 ‰ (Flude et al., 2016; Flude et al., 2017). Isotope fractionation during dissolution of CO_2 to form DIC is likely to produce $\delta^{13}C_{DIC}$ values up to ~10 ‰ higher than the original CO_2, see above) (Clark and Fritz, 1997). Thus, the lower $\delta^{13}C_{CO2}$ values that may be more typical of captured and injected CO_2, are more likely to produce DIC with $\delta^{13}C$ values that are difficult to distinguish from baseline $\delta^{13}C_{DIC}$ of seawater.

Compared to carbon isotopes, oxygen isotope equilibration times are much slower. At in-situ conditions of ~7 °C the equilibration between $\delta^{18}O_{CO2}$ and $\delta^{18}O_{H2O}$ would take ~40 hrs (Beck et al., 2005). When fully equilibrated with $\delta^{18}O_{H2O}$, the $\delta^{18}O_{CO2}$ would have reached a value of $\delta^{18}O_{CO2}$ = 44.8 ‰ (Brenninkmeijer et al., 1983). This slow equilibration process may be useful for assessing the time since the injected $CO_2(g)$ was in contact with seawater. However, the variability seen in $\delta^{18}O_{CO2}$

rig samples (S4, Supplementary Material) suggested that storage time (and thus continuing oxygen isotope fractionation between CO_2 and (condensed) H_2O vapour) in the gas sampler had a considerable impact on the $\delta^{18}O_{CO2}$ signature. This indicates that short storage times are crucial for use of $\delta^{18}O_{CO2}$ as a tracer, which may be difficult to achieve in an offshore setting and may limit the utility of $\delta^{18}O_{CO2}$ as a tracer.

To detect changes in the $\delta^{18}O_{DIC}$ signature in pore water and bottom water, an analytical procedure that is used on freshwater samples was tested in preparation for this study. This procedure is based on precipitating the DIC in the form of $SrCO_3$ (Beck et al., 2005; Dreybrodt et al., 2016). However, due to high dissolved sulphate (SO_4^{2-}) concentrations compared to DIC in seawater, most of the precipitate was composed of $SrSO_4$ rather than $SrCO_3$ (verified by SEM-EDS) and consequently the associated CO_2 signal of the acidified precipitate was too low for isotopic analysis on the mass spectrometer. Thus, this procedure was deemed impractical for this study, mainly due to restrictions in obtainable sample volume and thus precipitate. However, this method may still be useful at very high DIC concentrations and if one is not limited by sample volume. In regards to $\delta^{18}O_{H2O}$, the results suggest that $\delta^{18}O_{H2O}$ is not a sensitive tracer for CO_2 attribution and detection at the seafloor at the tested injection rates. Despite distinct differences between the isotopic signatures of the injected CO_2 ($\delta^{18}O_{CO2}$ = 32.5 ‰) and the pore waters ($\delta^{18}O_{H2O}$ = ~0.2 ‰) and bottom seawater ($\delta^{18}O_{H2O}$ = ~0.3 ‰), the CO_2 injection rates and associated leakage rates were volumetrically too low to be reflected in detectable changes of $\delta^{18}O_{H2O}$ in pore water and in bottom water. However, for geological CO_2 storage, large amounts of CO_2 are injected into a confined reservoir, and therefore CO_2 becomes a major oxygen source, which is reflected in shifts in the $\delta^{18}O$ values of both CO_2 and H_2O. Thus, the oxygen isotopic composition of injected CO_2 and reservoir fluids has been used successfully for in-reservoir monitoring, e.g., for quantifying the amount of CO_2 sequestered in the reservoir and for assessing CO_2-fluid-rock interactions (Johnson and Mayer, 2011; Johnson et al., 2011; Serno et al., 2016; Khararka et al., 2006). The findings of this study are in line with other studies (Roberts et al., 2017; Flude et al., 2016; Shevalier et al., 2014; Myrttinen et al., 2010) indicating that the utility of $\delta^{18}O$ tracer is primarily restricted to in-reservoir monitoring.

4.2. Quantification of CO_2 dissolution in pore water and leakage rate during the STEMM-CCS release experiment

In the event of unintended leakage of CO_2 from a storage reservoir, the ability to quantify the rate and spatial extent of a leak is essential to enable informed operational decisions and to minimise risk to the environment (EU, 2009). In this study, the fate of the injected CO_2 was quantified in two ways. Firstly, the leakage rate of free gas was quantified directly using the inverted funnel technique. The difference between the total injected CO_2 and the total leakage rate can be assumed to represent CO_2 that was retained in the sediment. This CO_2 may consist of both dissolved and gaseous CO_2. Secondly, the degree of CO_2 dissolution into the sediment pore water was quantified using low-solubility tracer gases added to the injected CO_2.

Overall, total leakage rates increased gradually from a minimum of ~1.3 kg CO_2 d^{-1} at the lowest injection rate (6 kg d^{-1}) to a maximum of ~70 kg CO_2 d^{-1} at the highest injection rate (143 kg d^{-1}) (Table 2, Fig. 5). The temporal variability of leakage rates during periods of constant injection flow rate were relatively small except for the 86 kg d^{-1} CO_2 injection period, when leakage rates varied by a factor of ~3, i.e., they dropped from ~50 kg d^{-1} on $D+7$ to 21 kg d^{-1} on $D+8$ and then rose to 61 kg d^{-1} the same day. Gas sampling was usually done from more intense seeps, suggesting that this variability was not a sampling artefact. When leakage rates dropped to 21 kg d^{-1}, the CH_4-based CO_2 dissolution estimates versus the amount of overall CO_2 retainment suggest that more CO_2 was retained in gaseous form than usual (Fig. 5). The temporal evolution of gas migration based on seismic surveys (carried out on $D+3$, $D+6$, $D+9$ and $D+16$) indicate that after $D+6$ gas
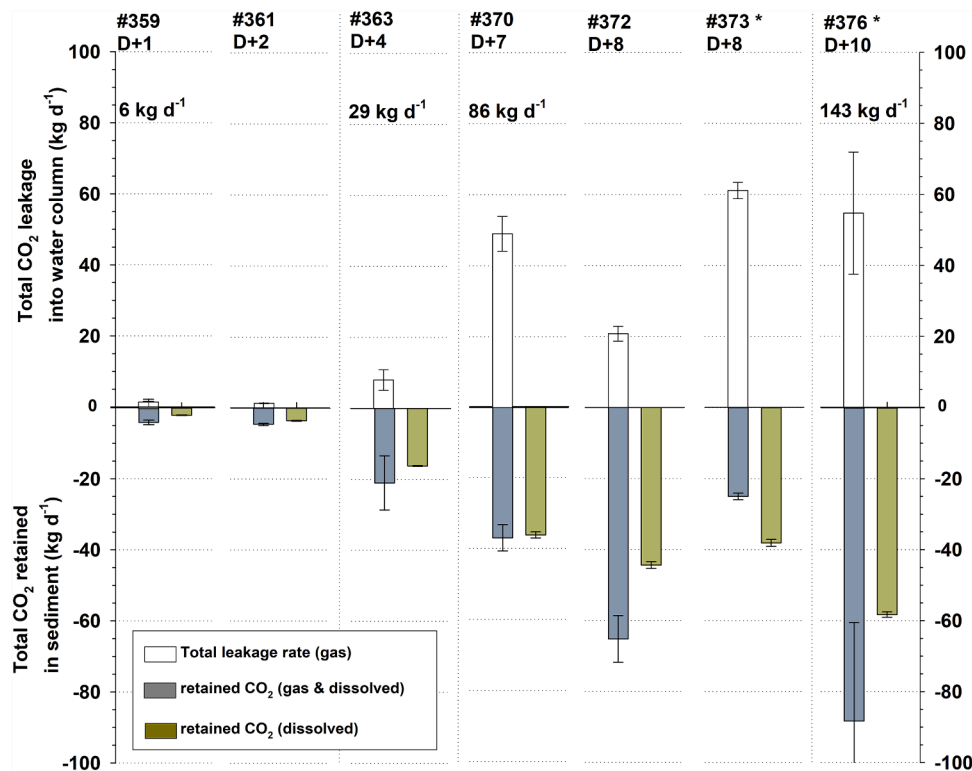
Fig. 5. Comparison of total leakage rates derived from direct inverted funnel measurements (white) and resulting amount of CO_2 that was retained in the sediment (gaseous and dissolved) (grey) versus CH_4-based estimate of CO_2 dissolution in the sediment (green). *same seep sampled on consecutive days. (For interpretation of the references to colour in this figure legend, the reader is referred to the web version of this article.)

started pooling in the sediment and had formed a detectable gas pocket in the subsurface by $D+9$, which was eventually connected to the seabed via relatively long-lived fluid escape features (chimneys) (Roche et al., 2021). This interpretation is supported by the variability of the funnel-based leakage rates observed during the 86 kg CO_2 d^{-1} injection period. Furthermore, the increase of leakage to 61 kg d^{-1} was associated with a CH_4-based CO_2 dissolution estimate that exceeds the total CO_2 retained (as gaseous and dissolved), likely caused by the delay in CO_2 leakage due to the formation of the gas pocket causing the "excess" CO_2 dissolution. However, it also indicates that the formation of the gas pocket causes a delay of CO_2 leakage across the seabed, which complicates direct referencing of leakage rates to injection flow rates.

Funnel-based leakage rates measured on $D+9$ and $D+10$ (143 kg CO_2 d^{-1} injection level) correspond to 38±12 and 48±7 % of the injected CO_2, which is within the range of leakage rates derived from passive acoustic measurements (22–62 %) (Li et al., 2021), from a combination of towed sensors and numerical simulations (64 %) (Gros et al., 2021) and is comparable with leakage rates derived by Eddy co-variance techniques (53–74 %) (Koopmans et al., submitted for publication). Given the variability of leakage and that none of these methods was tested at exactly the same time during the 143 kg CO_2 d^{-1} injection period, the funnel-derived leakage rates appear to be representative both temporally and quantitatively.

The range of funnel-based leakage rates indicates that 4.7 kg CO_2 d^{-1} at the lowest injection rate to 73 kg CO_2 d^{-1} at the highest injection rate were retained in the sediment, both in dissolved and gaseous form. The CH_4-based estimates of CO_2 dissolution in sediment pore water suggest that ~2 kg d^{-1} at the lowest injection flow rate to 60 kg d^{-1} at the highest injection flow rate dissolved in the pore water (Table 3). The changes in $\delta^{13}C_{CO2}$ isotopic composition between rig and seep gas samples indicate less CO_2 dissolution into pore water of ~1.3 kg d^{-1} (~22 %) and 38 kg d^{-1} (~27 %), respectively (S6, Supplementary Material). This is likely caused by more complex boundary conditions present in the pore water

than the simplified assumptions made for the TAMOC simulation of ^{12}C and ^{13}C mass transfer. Interpolated over the period from $D+1$ to $D+10$, when the last gas samples were taken, the funnel-based leakage rates add up to a total leakage of ~250 kg CO_2, which corresponds to ~43 % of the total amount of CO_2 injected until $D+10$ (~580 kg CO_2). This suggests that ~330 kg CO_2 were retained in the sediment, both in dissolved and gaseous form. The CH_4-based estimates suggest that over this period ~257 kg CO_2 dissolved into sediment pore water indicating that the remainder of ~73 kg CO_2 was present in the sediment as free gas until $D+10$. This is comparable to the estimate of ~91 kg of free gas contained in the gas pocket based on the seismic survey conducted on $D+9$ (Roche et al., 2021).

In a real-world scenario, leakage is unlikely to be diffuse across the whole reservoir area but rather focussed, e.g., through small fractures and faults or through poorly-sealed, abandoned wells (IPCC, 2005; Miocic et al., 2016; Alcalde et al., 2018). Applying an acceptable terrestrial leakage rate of 0.01 % reservoir loss per year (e.g., Hepple and Benson, 2005; Chadwick et al., 2008; Haugan, 2020) to the injection of 1 Mt CO_2 yr^{-1} over 20 years that was projected for the Goldeneye reservoir (Dean and Tucker, 2017), corresponds to acceptable leakage rates of 274 kg d^{-1} after the first year of injection and 5480 kg d^{-1} after 20 years of injection when full storage capacity is reached. During the controlled CO_2 release experiment a total of 675 kg of CO_2 were injected into the shallow sediment at 3 mbsf for 11 days. The maximum funnel-based leakage rate of gaseous CO_2 across the seabed was ~70 kg CO_2 d^{-1}, i. e., much lower than the above range of acceptable leakage rates. In addition, the depth of CO_2 release within the sediments was substantially shallower than any proposed sub-seafloor storage reservoir. However, both the flow rates and the type (point-release) of the simulated leakage are relevant for real-world scenarios. The methods tested here provided a realistic quantitative estimate of the fate of CO_2 and agreed well with other estimates at relevant injection flow rates that are below the threshold, that would present an environmental risk

(Blackford et al., 2020).

4.3. Use of tracers for environmental monitoring of offshore CO₂ storage

As most tracer studies have been performed in onshore settings, the applicability of tracers in offshore marine environments, tracer behaviour, and utility in the marine environment are currently poorly known. Amongst the main uncertainties are CO_2-tracer behaviour and methods for detecting and sampling tracers in the marine environment (Roberts et al., 2017).

As mentioned earlier, the selection of tracers used in this study was based on previous work (Roberts et al., 2017; Myers et al., 2013 and references therein; Flude et al., 2016; Dean and Tucker, 2017) but was also largely determined by the underlying experimental setup and aspects of tracer availability, analytical feasibility and associated costs.

The STEMM-CCS experiment principally focused on assessing the behaviour and utility of tracers in the gas phase, which is why low solubility tracers were used. Analyses of tracers in the dissolved phase would require addition of tracers with higher solubility, as well as the capability to either (i) measure the dissolved tracer in-situ or (ii) to take discrete water samples and maintain them at in-situ pressure and temperature conditions until they can be analysed. Progress in the field of underwater mass spectrometry now permits in-situ measurements of a range of dissolved gases and stable isotopes but to date these instruments are highly specialised and are not commercially available (Chua et al., 2016 and references therein). The capability to retrieve and maintain discrete water samples at in-situ conditions has been demonstrated in the marine environment (e.g., Zhu et al., 2011; Brennwald et al., 2003; Garel et al., 2019; Bianchi et al., 1999; Gardner and Solomon, 2009), but has significant time and space demands for ROV sampling, and is expensive. These constraints may limit the utility of these studies for operational monitoring. Another difficulty of using dissolved tracers as a diagnostic tool for CO_2 leakage are differences in the physical properties of tracers and CO_2. For instance, models that simulate the rise of gas bubbles and the associated dissolution of CO_2 and tracers from the gas bubble into the fluid phase show that, as a result of differences in solubility, concentrations of tracers in the dissolved phase will continue to increase while most of the CO_2 has dissolved already (Gros et al., 2021).

Sampling and analysis of tracers in the gas phase required the use of specialised equipment and techniques. For gas bubble sampling, custom-made GBS (Corsyde, Germany) were successfully operated by the ROV manipulator arms. A few gas samples were lost due to (i) overtightening of the ball valve mechanism when closing the GBS, which led to gas loss from the sampler during ascent and (ii) loss of the inverted funnels during GBS handling, which made gas sampling impossible. Thus, for sampling involving the ROV, equipment needs to be as sturdy as possible. The analytical setup for onboard analysis of C_3F_8, SF_6, CH_4 and CO_2 using a custom-built sample injection system allowed for analysis of the gas composition in less than 30 min after recovery of the samples demonstrating that the analytical part of the source attribution from gas samples can be done quickly. For storage of gas samples pre-evacuated 12 mL Exetainers® with double wadded septa (Labco) proved useful (S2, Supplementary Material). The mass spectrometer used for Kr analysis (Section 2.3.1.3.) was not available for onboard measurements during the release experiment but is portable and thus practical for onboard analysis of discrete gas samples. As part of this study, a measurement protocol for Kr quantification was developed (S2, Supplementary Material). This protocol could be adapted for other gas species of interest, e.g., xenon isotopes that were identified as potentially suitable tracers in a feasibility study for a proposed measurement, monitoring and verification (MMV) programme at Goldeneye (Dean and Tucker, 2017).

CO_2 in sub-seabed storage reservoirs may partly or completely dissolve into formation waters, such that any leakage from the reservoir is likely to result in displacement of pore waters from the sedimentary overburden prior to the escape of CO_2. Thus, leakage may first be detected by the presence of displaced deep (anoxic) pore waters or Cl- and gas-rich formation waters, rather than a CO_2 anomaly. Analyses of sediment pore waters during the release experiment have shown that dissolution of CO_2 into pore water raised pore water temperature and altered pore water geochemistry (de Beer et al., 2021; Lichtschlag et al., 2021) emphasising the importance of precursor indicators of leakage for monitoring (Lichtschlag et al., submitted for publication). A prerequisite of the quantification technique used in this study is knowledge of the initial CO_2:tracer ratio in the injection gas. Maintaining the stability of tracer injection into the main CO_2 gas stream at low flow rates proved difficult (S3, Supplementary Material). This meant that a rig gas sample had to be taken during every sampling campaign in order to quantify CO_2 dissolution in sediment pore waters. In a real-world scenario CO_2: tracer variability across the migration pathway will likely be a challenge too. In the event of an unintended leakage of CO_2 from the storage reservoir, e.g., through faults, fractures or through leaking wells, the CO_2 and tracers will be exposed to changing physico-chemical conditions and will undergo aqueous dissolution over hundreds to thousands of meters of vertical ascent. At Goldeneye reservoir conditions (83 °C and 220–260 bar and at ~2500 mbsf) (Shell, 2015)), pure CO_2, Kr, SF_6, and C_3F_8 would be in a supercritical state (Poling et al., 2001). The behaviours of leaking fluids during ascent from a reservoir to the seafloor are complex and depend on changing conditions of pressure, temperature, and composition (modified through aqueous dissolution). During ascent to the seabed, the initially single-phase mixture (at reservoir conditions) may pass through a two-phase region and finally transition to pure gas before emerging from the seafloor. These processes will control the composition of the gas and fluids that escape from the seabed into the overlying water column. The use of tracers as a diagnostic tool thus relies (i) on modelling of subsurface CO_2 and tracer migration through the overburden, and (ii) on robust knowledge of the tracer properties and migration behaviour as a function of the changing physico-chemical conditions. The coupling of tracer data with reactive-transport modelling allows reservoir and overburden properties and transport processes (advection, diffusion) to be taken into account, and characterisation of reactive processes at the CO_2-pore fluid/brine interface as they evolve during CO_2 migration (Cohen et al., 2013; Gasparini et al., 2015; Tong et al., 2013; Soltanian et al., 2018). Laboratory experiments designed to study tracer versus CO_2 migration, tracer partitioning and fluid flow under controlled physico-chemical conditions through different types of porous media (Kilgallon et al., 2018; Zhong et al., 2014; Reynolds et al., 2017; Myers et al., 2012; Myers et al., 2013) will be crucial for parameterising these models. However, given the complexity associated with the use of tracers, their utility in a real-world scenario will likely be limited to attribution purposes rather than leakage quantification at the seafloor.

5. Conclusions

The STEMM-CCS project completed a large-scale field experiment in the central North Sea designed to simulate and detect an unintended emission of CO_2 from a sub-seabed CO_2 storage site. To field-test a variety of leak detection and quantification techniques, 675 kg of CO_2 was injected into the sub-seabed sediments at rates of between 6 and 143 kg CO_2 d^{-1}. A set of natural, inherent tracers (^{13}C, ^{18}O) of injected CO_2 and non-toxic added tracer gases (C_3F_8, SF_6, Kr, inherent CH_4) were assessed for their ability to (i) attribute the source of the CO_2 and (ii) quantify CO_2 fluxes across the seabed. Based on elevated DIC and $\delta^{13}C_{DIC}$, the presence of injected CO_2 in sediment pore waters and the water column was successfully detected at flow rates of 6 kg CO_2 d^{-1} and 29 kg CO_2 d^{-1}, respectively. In contrast, CO_2 leakage could not be detected in the $\delta^{18}O_{H2O}$ signature of both sediment pore water samples and water column samples. Trace gas analyses suggest that the amount of CO_2 retained in the sediment due to dissolution in pore water ranged from 35 % at the lowest injection rate (6 kg CO_2 d^{-1}) to 41 % at the highest

injection rate (143 kg CO_2 d^{-1}). Leakage rates derived from observations and measurements of bubble seeps at the seabed showed that the total leakage rates ranged from 22 % at the lowest injection rate to 48 % of injected CO_2 at the highest injection rate. The gas sampling and analytical methods tested proved effective for quick onboard source attribution. If most of the injected CO_2 dissolves in sediment pore waters, i.e., in the absence of gas bubble seeps at the seabed, detection of injected CO_2 via DIC anomalies and tracers would be better done using in-situ techniques rather than discrete water sampling. Discrete water sampling is further complicated by the need to maintain samples at in-situ temperature and pressure to minimise degassing.

Declaration of Competing Interest

The authors declare that they have no known competing financial interests or personal relationshipsthat could have appeared to influence the work reported in this paper.

CRediT authorship and contribution statement

Conceptualisation and management of overall project: JMM, RHJ, KS, DC and AL.

Design and implementation of experimental work: AF, JMM, RHJ, KS and RB.

Investigation, laboratory analysis, methdology: AF, KS, RB, CJB, DC, CD, SF, JG, DJH, AL, CRP, KP, JS and RLT.

AF led the writing of the paper; contributions to writing and revising were also provided by all co-authors.

Supplementary materials

Supplementary material associated with this article can be found, in the online version, at doi:10.1016/j.ijggc.2021.103421.

References

Alcalde, J., Flude, S., Wilkinson, M., Johnson, G., Edlmann, K., Bond, C.E., Scott, V., Gilfillan, S.M.V., Ogaya, X., Haszeldine, R.S., 2018. Estimating geological CO2 storage security to deliver on climate mitigation. Nat. Commun. 9, 2201. https://doi.org/10.1038/s41467-018-04423-1.

Assayag, N., Rivé, K., Ader, M., Jézéquel, D., Agrinier, P., 2006. Improved method for isotopic and quantitative analysis of dissolved inorganic carbon in natural water samples. Rapid Commun. Mass Spectrom. 20, 2243–2251. https://doi.org/10.1002/rcm.2585.

Assayag, N., Matter, J.M., Ader, M., Goldberg, D., Agrinier, P., 2009. Water-rock interactions during a CO2 injection field-test: implications on host rock dissolution and alteration effects. Chem. Geol. 265, 227–235. https://doi.org/10.1016/j.chemgeo.2009.02.007.

Beck, W.C., Grossman, E.L., Morse, J.W., 2005. Experimental studies of oxygen isotope fractionation in the carbonic acid system at 15°, 25°, and 40 °C. Geochim. Cosmochim. Acta 69, 3493–3503. https://doi.org/10.1016/j.gca.2005.02.003.

Bianchi, A., Garcin, J., Tholosan, O., 1999. A high-pressure serial sampler to measure microbial activity in the deep sea. Deep Sea Res. Part I 46, 2129–2142. https://doi.org/10.1016/S0967-0637(99)00039-4.

Blackford, J., Stahl, H., Bull, J.M., Bergès, B.J.P., Cevatoglu, M., Lichtschlag, A., Connelly, D., James, R.H., Kita, J., Long, D., Naylor, M., Shitashima, K., Smith, D., Taylor, P., Wright, I.C., Akhurst, M., Chen, B., Gernon, T.M., Hauton, C., Hayashi, M., Kaieda, H., Leighton, T.G., Sato, T., Sayer, M.D.J., Suzumura, M., Tait, K., Vardy, M.E., White, P.R., Widdicombe, S., 2014. Detection and impacts of leakage from sub-seafloor deep geological carbon dioxide storage. Nat Clim Chang 1–6. https://doi.org/10.1038/NCLIMATE2381.

Blackford, J., Bull, J.M., Cevatoglu, M., Connelly, D., Hauton, C., James, R.H., Lichtschlag, A., Stahl, H., Widdicombe, S., Wright, I.C., 2015. Marine baseline and monitoring strategies for carbon dioxide capture and storage (CCS). Int. J. Greenhouse Gas Control 38, 221–229. https://doi.org/10.1016/j.ijggc.2014.10.004.

Blackford, J., Artioli, Y., Clark, J., de Mora, L., 2017. Monitoring of offshore geological carbon storage integrity: implications of natural variability in the marine system and the assessment of anomaly detection criteria. Int. J. Greenhouse Gas Control 64, 99–112. https://doi.org/10.1016/j.ijggc.2017.06.020.

Blackford, J., Alendal, G., Avlesen, H., Cazenave, P.W., Chen, B., Dewar, M., Holt, J.T., Phelps, J., 2020. Impact and detectability of hypothetical CCS offshore seep scenarios as an aid to storage assurance and risk assessment. Int. J. Greenhouse Gas Control 95. https://doi.org/10.1016/j.ijggc.2019.102949, 10.1016/j.ijggc.2019.102949.

Boreham, C., Underschultz, J., Stalker, L., Kirste, D., Freifeld, B., Jenkins, C., Ennis-King, J., 2011. Monitoring of CO2 storage in a depleted natural gas reservoir: gas geochemistry from the CO2CRC Otway Project. Australia International Journal of Greenhouse Gas Control 5, 1039–1054. https://doi.org/10.1016/j.ijggc.2011.03.011.

Bottinga, Y., 1968. Calculation of fractionation factors for carbon and oxygen isotopic exchange in the system calcite-carbon dioxide-water. J. Phys. Chem. 72, 800–808. https://doi.org/10.1021/j100849a008.

Böttner, C., Berndt, C., Reinardy, B.T.I., Geersen, J., Karstens, J., Bull, J.M., Callow, B.J., Lichtschlag, A., Schmidt, M., Elger, J., Schramm, B., Haeckel, M., 2019. Pockmarks in the Witch Ground Basin, Central North Sea, Geochemistry, Geophysics. Geosystems 20, 1698–1719. https://doi.org/10.1029/2018GC008068.

Brenninkmeijer, C.A.M., Kraft, P., Mook, W.G., 1983. Oxygen isotope fractionation between CO2 and H2O. Chem. Geol. 41, 181–190. https://doi.org/10.1016/S0009-2541(83)80015-1.

Brennwald, M.S., Hofer, M., Peeters, F., Aeschbach-Hertig, W., Strassmann, K., Kipferl, R., Imboden, D.M., 2003. Analysis of dissolved noble gases in the porewater of lacustrine sediments. Limnology and Oceanography: Methods 1, 51–62. https://doi.org/10.4319/lom.2003.1.51.

Brennwald, M.S., Schmidt, M., Oser, J., Kipfer, R., 2016. A Portable and Autonomous Mass Spectrometric System for On-Site Environmental Gas Analysis. Environ. Sci. Technol. 50, 13455–13463. https://doi.org/10.1021/acs.est.6b03669.

Cevatoglu, M., Bull, J.M., Vardy, M.E., Gernon, T.M., Wright, I.C., Long, D., 2015. Gas migration pathways, controlling mechanisms and changes in sediment acoustic properties observed in a controlled sub-seabed CO2 release experiment. Int. J. Greenhouse Gas Control 38, 26–43. https://doi.org/10.1016/j.ijggc.2015.03.005.

Chadwick, A., Arts, R., Bernstone, C., May, F., Thibeau, S., Zweigel, P., 2008. Best Practice For the Storage of CO2 in Saline Aquifers - Observations and Guidelines from the SACS and CO2STORE Projects. Nottingham: British Geological Survey Occasional Publication No. 14, Keyworth.

Chand, S., Crémière, A., Lepland, A., Thorsnes, T., Brunstad, H., Stoddart, D., 2017. Long-term fluid expulsion revealed by carbonate crusts and pockmarks connected to subsurface gas anomalies and palaeo-channels in the central North Sea. Geo Mar. Lett. 37, 215–227. https://doi.org/10.1007/s00367-016-0487-x.

Chua, E.J., Savidge, W., Short, R.T., Cardenas-Valencia, A.M., Fulweiler, R.W., 2016. A Review of the Emerging Field of Underwater Mass Spectrometry. Front Mar Sci 3. https://doi.org/10.3389/fmars.2016.00209.

Clark, I.D., Fritz, P., 1997. Environmental Isotopes in Hydrogeology. CRC Press, 1st ed.

Cohen, G., Loisy, C., Laveuf, C., Le Roux, O., Delaplace, P., Magnier, C., Rouchon, V., Garcia, B., Cerepi, A., 2013. The CO2-Vadose project: experimental study and modelling of CO2 induced leakage and tracers associated in the carbonate vadose zone. Int. J. Greenhouse Gas Control 14, 128–140. https://doi.org/10.1016/j.ijggc.2013.01.008.

Connelly, D., 2019. JC180 Cruise report- Strategies for the Environmental Monitoring of Marine Carbon Capture and Storage. STEMM-CCS April 25th 2019 - May 30th 2019 Southampton - Aberdeen - Southampton. National Oceanography Centre, Southampton, UK.

Dale, A.W., Sommer, S., Lichtschlag, A., Koopmans, D., Haeckel, M., Kossel, E., Deusner, C., Linke, P., Scholten, J., Wallmann, K., van Erk, M.R., Gros, J., Scholz, F., Schmidt, M., 2021. Defining a biogeochemical baseline for sediments at Carbon Capture and Storage (CCS) sites: an example from the North Sea (Goldeneye). Int. J. Greenhouse Gas Control 106, 103265. https://doi.org/10.1016/j.ijggc.2021.103265.

de Beer, D., Lichtschlag, A., Flohr, A., van Erk, M.R., Ahmerkamp, S., Holtappels, M., Haeckel, M., Strong, J., 2021. Sediment acidification and temperature increase in an artificial CO2 vent. Int. J. Greenhouse Gas Control 105, 103244. https://doi.org/10.1016/j.ijggc.2020.103244.

Dean, M., Tucker, O., 2017. A risk-based framework for Measurement, Monitoring and Verification (MMV) of the Goldeneye storage complex for the Peterhead CCS project, UK. Int. J. Greenhouse Gas Control 61, 1–15. https://doi.org/10.1016/j.ijggc.2017.03.014.

Dickson, A.G., Sabine, C.L., Christian, J.R., 2007. Guide to Best Practices for Ocean CO2 Measurements. PICES Special Publication 3. https://www.ncei.noaa.gov/acce ss/ocean-carbon-data-system/oceans/Handbook_2007/Guide_all_in_one.pdf.

Dissanayake, A.L., Gros, J., Socolofsky, S.A., 2018. Integral models for bubble, droplet, and multiphase plume dynamics in stratification and crossflow. Environ. Fluid Mech. 18, 1167–1202. https://doi.org/10.1007/s10652-018-9591-y.

Dixon, T., Romanak, K., 2015. Improving monitoring protocols for CO2 geological storage with technical advances in CO$_2$ attribution monitoring. Int. J. Greenhouse Gas Control 41, 29–40. https://doi.org/10.1016/j.ijggc.2015.05.029.

Dlugokencky, E.J., Mund, J.W., Crotwell, A.M., Crotwell, M.J., Thoning, K.W.: Atmospheric Carbon Dioxide Dry Air Mole Fractions from the NOAA GML Carbon Cycle Cooperative Global Air Sampling Network, 1968-2019, Version: 2021-02, https://doi.org/10.15138/wkgj-f215, last accessed: 1 May 2020. 2020.

Dreybrodt, W., Hansen, M., Scholz, D., 2016. Processes affecting the stable isotope composition of calcite during precipitation on the surface of stalagmites: laboratory experiments investigating the isotope exchange between DIC in the solution layer on top of a speleothem and the CO2 of the cave atmosphere. Geochim. Cosmochim. Acta 174, 247–262. https://doi.org/10.1016/j.gca.2015.11.012.

EIGA: Carbon dioxide food and beverages grade, source qualification, quality standards and verification. European Industrial Gases Association AISBL. EIGA Doc 70/17, 2016.

EU, 2009. Implementation of Directive 2009/31/EC on the Geological Storage of Carbon Dioxide, Guidance Documents 1-4. European Commission. https://ec.europa. eu/clima/policies/innovation-fund/ccs/implementation_en#tab-0-1.

Flohr, A., Schaap, A., Achterberg, E.P., Alendal, G., Arundell, M., Berndt, C., Blackford, J., Böttner, C., Borisov, S.M., Brown, R., Bull, J.M., Carter, L., Chen, B., Dale, A.W., de Beer, D., Dean, M., Deusner, C., Dewar, M., Durden, J.M., Elsen, S., Esposito, M., Faggetter, M., Fischer, J.P., Gana, A., Gros, J., Haeckel, M., Hanz, R., Holtappels, M., Hosking, B., Huvenne, V.A.I., James, R.H., Koopmans, D., Kossel, E., Leighton, T.G., Li, J., Lichtschlag, A., Linke, P., Loucaides, S., Martínez-Cabanas, M., Matter, J.M., Mesher, T., Monk, S., Mowlem, M., Oleynik, A., Papadimitriou, S., Paxton, D., Pearce, C.R., Peel, K., Roche, B., Ruhl, H.A., Saleem, U., Sands, C., Saw, K., Schmidt, M., Sommer, S., Strong, J.A., Triest, J., Ungerböck, B., Walk, J., White, P., Widdicombe, S., Wilson, R.E., Wright, H., Wyatt, J., Connelly, D.P., 2021. Towards improved monitoring of offshore carbon storage: a real-world field experiment detecting a controlled sub-seafloor CO2 release. Int. J. Greenhouse Gas Control 106, 103237. https://doi.org/10.1016/j.ijggc.2020.103237.

Flude, S., Johnson, G., Gilfillan, S.M.V., Haszeldine, R.S., 2016. Inherent Tracers for Carbon Capture and Storage in Sedimentary Formations: composition and Applications. Environ. Sci. Technol. 50, 7939–7955. https://doi.org/10.1021/acs. est.6b01548, 10.1021/acs.est.6b01548.

Flude, S., Györe, D., Stuart, F.M., Zurakowska, M., Boyce, A.J., Haszeldine, R.S., Chalaturnyk, R., Gilfillan, S.M.V., 2017. The inherent tracer fingerprint of captured CO2. Int. J. Greenhouse Gas Control 65, 40–54. https://doi.org/10.1016/j. ijggc.2017.08.010.

Friedlingstein, P., Jones, M.W., O'Sullivan, M., Andrew, R.M., Hauck, J., Peters, G.P., Peters, W., Pongratz, J., Sitch, S., Le Quéré, C., Bakker, D.C.E., Canadell, J.G., Ciais, P., Jackson, R.B., Anthoni, P., Barbero, L., Bastos, A., Bastrikov, V., Becker, M., Bopp, L., Buitenhuis, E., Chandra, N., Chevallier, F., Chini, L.P., Currie, K.I., Feely, R. A., Gehlen, M., Gilfillan, D., Gkritzalis, T., Goll, D.S., Gruber, N., Gutekunst, S., Harris, I., Haverd, V., Houghton, R.A., Hurtt, G., Ilyina, T., Jain, A.K., Joetzjer, E., Kaplan, J.O., Kato, E., Klein Goldewijk, K., Korsbakken, J.I., Landschützer, P., Lauvset, S.K., Lefèvre, N., Lenton, A., Lienert, S., Lombardozzi, D., Marland, G., McGuire, P.C., Melton, J.R., Metzl, N., Munro, D.R., Nabel, J.E.M.S., Nakaoka, S.I., Neill, C., Omar, A.M., Ono, T., Peregon, A., Pierrot, D., Poulter, B., Rehder, G., Resplandy, L., Robertson, E., Rödenbeck, C., Séférian, R., Schwinger, J., Smith, N., Tans, P.P., Tian, H., Tilbrook, B., Tubiello, F.N., van der Werf, G.R., Wiltshire, A.J., Zaehle, S., 2019. Global Carbon Budget. Earth Syst. Sci. Data 11, 1783–1838. https://doi.org/10.5194/essd-11-1783-2019, 10.5194/essd-11-1783-2019, 2019.

Furre, A.-.K., Eiken, O., Alnes, H., Vevatne, J.N., Kiær, A.F., 2017. 20 Years of Monitoring CO2-injection at Sleipner. Energy Procedia 114, 3916–3926. https://doi.org/ 10.1016/j.egypro.2017.03.1523.

Gardner, P., Solomon, D.K., 2009. An advanced passive diffusion sampler for the determination of dissolved gas concentrations. Water Resour. Res. 45 https://doi. org/10.1029/2008WR007399.

Garel, M., Bonin, P., Martini, S., Guasco, S., Roumagnac, M., Bhairy, N., Armougom, F., Tamburini, C., 2019. Pressure-Retaining Sampler and High-Pressure Systems to Study Deep-Sea Microbes Under in situ Conditions. Front Microbiol 10. https://doi. org/10.3389/fmicb.2019.00453.

Gasparini, A., Credoz, A., Grandia, F., Garcia, D.A., Bruno, J., 2015. Experimental and numerical modeling of CO2 leakage in the vadose zone. Greenhouse Gases: Science and Technology 5, 732–755. https://doi.org/10.1002/ghg.1523.

Gilfillan, S., Haszeldine, R.S., Györe, D., Kilgallon, R., Wilkinson, M., 2014. The application of noble gases and carbon stable isotopes in tracing the fate, migration and storage of CO2. Energy Procedia 63, 4123–4133. https://doi.org/10.1016/j. egypro.2014.11.443.

Gros, J., Reddy, C.M., Nelson, R.K., Socolofsky, S.A., Arey, J.S., 2016. Simulating Gas-Liquid−Water Partitioning and Fluid Properties of Petroleum under Pressure: implications for Deep-Sea Blowouts. Environ. Sci. Technol. 50, 7397–7408. https:// doi.org/10.1021/acs.est.5b04617, 10.1021/acs.est.5b04617.

Gros, J., Schmidt, M., Linke, P., Dötsch, S., Triest, J., Martínez-Cabanas, M., Esposito, M., Dale, A.W., Sommer, S., Flohr, A., Fone, J., Bull, J.M., Roche, B., Strong, J., Saw, K., Brown, R., Koopmans, D., Schaap, A., Wallmann, K., 2021. Quantification of dissolved CO2 plumes at the Goldeneye CO2-release experiment. Int. J. Greenhouse Gas Control. https://doi.org/10.1016/j.ijggc.2021.103387 this issue.

Gros, J., Socolofsky, S.A., Dissanayake, A.L., Jun, I., Zhao, L., Boufadel, M.C., Reddy, C. M., Arey, J.S., 2017. Petroleum dynamics in the sea and influence of subsea dispersant injection during Deepwater Horizon. Proc. Natl Acad. Sci. 114, 10065. https://doi.org/10.1073/pnas.1612518114.

Gros, J., Schmidt, M., Dale, A.W., Linke, P., Vielstädte, L., Bigalke, N., Haeckel, M., Wallmann, K., Sommer, S., 2019. Simulating and Quantifying Multiple Natural Subsea CO2 Seeps at Panarea Island (Aeolian Islands, Italy) as a Proxy for Potential Leakage from Seabed Carbon Storage Sites. Environmental Science & Technology 53. https://doi.org/10.1021/acs.est.9b02131.

Györe, D., Stuart, F.M., Gilfillan, S.M.V., Waldron, S., 2015. Tracing injected CO2 in the Cranfield enhanced oil recovery field (MS, USA) using He, Ne and Ar isotopes. Int. J. Greenhouse Gas Control 42, 554–561. https://doi.org/10.1016/j.ijggc.2015.09.009.

Györe, D., Gilfillan, S., Stuart, F.M., 2017. Tracking the interaction between injected CO2 and reservoir fluids using noble gas isotopes in an analogue of large-scale carbon capture and storage. Appl. Geochem. 78, 116–128. https://doi.org/10.1016/j. apgeochem.2016.12.012.

Hansen, O., Gilding, D., Nazarian, B., Osdal, B, Ringrose, P., Kristoffersen, J.-B., Eiken, O., Hansen, H., 2013. Snøhvit: The History of Injecting and Storing 1 Mt CO2 in the Fluvial Tubåen Fm. Energy Procedia 37, 3565–3573. https://doi.org/ 10.1016/j.egypro.2013.06.249.

Haszeldine, R.S., Flude, S., Johnson, G., Scott, V., 2018. Negative emissions technologies and carbon capture and storage to achieve the Paris Agreement commitments. Philos. Trans. R. Soc., A 376, 20160447. https://doi.org/10.1098/rsta.2016.0447.

Haugan, P.M., Joos, F., 2020. Metrics to assess the mitigation of global warming by carbon capture and storage in the ocean and in geological reservoirs. Geophys. Res. Lett. 31, 10.1029/2004GL020295, 2004.

Hepple, R.P., Benson, S.M., 2005. Geologic storage of carbon dioxide as a climate change mitigation strategy: performance requirements and the implications of surface seepage. Environ. Geol. 47, 576–585. https://doi.org/10.1007/s00254-004-1181-2.

IEAGHG, 2008. Assessment of Sub Sea Ecosystem Impacts. EA Greenhouse Gas R&D programme (IEAGHG). https://www.ieaghg.org/docs/General_Docs/Reports/200 8-08.pdf.

IMO, 2006. Amendment of 1996 Protocol to the Convention on the Prevention of Marine Pollution by Dumping of Wastes and other Matter, 1972. International Maritime Organization. http://www.imo.org/en/OurWork/Environment/LCLP/Pages/def ault.aspx.

IPCC, 2005. Special Report on Carbon Dioxide Capture and Storage. Prepared by Working Group III of the Intergovernmental Panel on Climate Change. In: Metz, B., Davidson, O., de Coninck, H.C., Loos, M., Meyer, L.A. (Eds.), The Edinburgh Building Shaftesbury Road, Cambridge CB2 2RU ENGLAND. Cambridge University Press.

IPCC: Guidelines for National Greenhouse Gas Inventories, Vol. 2 Energy, Chapter 5 Carbon Dioxide Transport, Injection and Geological Storage. IGES, Japan, 2006.

IPCC, 2018. Summary for Policymakers. In: global Warming of 1.5 °C. In: Masson-Delmotte, V., Zhai, P., Pörtner, H.-O., Roberts, D., Skea, J., Shukla, P.R., et al. (Eds.), An IPCC Special Report On the Impacts of Global Warming of 1.5 °C Above Pre-Industrial Levels and Related Global Greenhouse Gas Emission pathways, in the Context of Strengthening the Global Response to the Threat of Climate change, Sustainable development, and Efforts to Eradicate Poverty. World Meteorological Organization, Geneva, Switzerland, p. 32 (eds.).

Jähne, B., Heinz, G., Dietrich, W., 1987. Measurement of the diffusion coefficients of sparingly soluble gases in water. Journal of Geophysical Research: Oceans 92, 10767–10776. https://doi.org/10.1029/JC092iC10p10767.

Jenkins, C., Chadwick, a., Hovorka, S.D., 2015. The state of the art in monitoring and verification—Ten years on. Int. J. Greenhouse Gas Control 40, 312–349. https://doi. org/10.1016/j.ijggc.2015.05.009.

Jenkins, C.R., Cook, P.J., Ennis-King, J., Underschultz, J., Boreham, C., Dance, T., de Caritat, P., Etheridge, D.M., Freifeld, B., Hortle, A., Kirste, D., Paterson, L., Pevzner, R., Schacht, U., Sharma, S., Stalker, L., Urosevic, M., 2012. Safe storage and effective monitoring of CO2 in depleted gas fields. Proc. Natl Acad. Sci. 109 https:// doi.org/10.1073/pnas.1107255108. E35-E41.

Johnson, G., Mayer, B., 2011. Oxygen isotope exchange between H2O and CO2 at elevated CO2 pressures: implications for monitoring of geological CO2 storage. Appl. Geochem. 26, 1184–1191. https://doi.org/10.1016/j.apgeochem.2011.04.007.

Johnson, G., Mayer, B., Nightingale, M., Shevalier, B., Hutcheon, I., 2011. Using oxygen isotope ratios to quantitatively assess trapping mechanisms during CO2 injection into geological reservoirs. The Pembina case study Chemical Geology 283, 185–193. https://doi.org/10.1016/j.chemgeo.2011.01.016.

Jones, D.G., Barkwith, A.K.A.P., Hannis, S., Lister, T.R., Gal, F., Graziani, S., Beaubien, S. E., Widory, D., 2014. Monitoring of near surface gas seepage from a shallow injection experiment at the CO2 Field Lab, Norway. Int. J. Greenhouse Gas Control 28, 300–317. https://doi.org/10.1016/j.ijggc.2014.06.021.

Judd, A.G., Long, D., Sankey, M., 1994. Pockmark formation and activity, UK block 15/ 25, North Sea. Bull. Geol. Soc. Den. 41, 34–49.

Jun, I., 2018. A Numerical Model For Hydrocarbon Bubbles from Natural Seeps Within Hydrate Stability Zone, Texas A&M University, College Station, Texas, Ph.D. Dissertation. Texas A&M University.

Karstens, J., Berndt, C., 2015. Seismic chimneys in the Southern Viking Graben - Implications for palaeo fluid migration and overpressure evolution. Earth Planet. Sci. Lett. 412, 88–100. https://doi.org/10.1016/j.epsl.2014.12.017.

Kharaka, Y.K., Cole, D.R., Hovorka, S.D., Gunter, W.D., Knauss, K.G., Freifeld, B.M., 2006. Gas-water-rock interactions in Frio Formation following CO2 injection: implications for the storage of greenhouse gases in sedimentary basins. Geology 34, 577–580. https://doi.org/10.1130/G22357.1.

Kilgallon, R., Gilfillan, S.M.V., Edlmann, K., McDermott, C.I., Naylor, M., Haszeldine, R. S., 2018. Experimental determination of noble gases and SF6, as tracers of CO2 flow

through porous sandstone. Chem. Geol. 480, 93–104. https://doi.org/10.1016/j.chemgeo.2017.09.022.

Kim, J., Yu, S., Yun, S.-.T., Kim, K.-.H., Kim, J.-.H., Shinn, Y.-.J., Chae, G., 2019. CO2 leakage detection in the near-surface above natural CO2-rich water aquifer using soil gas monitoring. Int. J. Greenhouse Gas Control 88, 261–271. https://doi.org/10.1016/j.ijggc.2019.06.015.

Kim, S.-.T., Coplen, T.B., Horita, J., 2015. Normalization of stable isotope data for carbonate minerals: implementation of IUPAC guidelines. Geochim. Cosmochim. Acta 158, 276–289. https://doi.org/10.1016/j.gca.2015.02.011.

Koopmans, D., Meyer, V., Holtappels, M., Schaap, A., Dewar, M., Färber, P., Long, M.H., Connelly, D.P., de Beer, D., n.d.. Detection and quantification of carbon dioxide gas at the seafloor using pH eddy covariance and measurements of plume advection. International Journal of Greenhouse Gas Control. Submitted for publication.

Lee, G.H., Lee, B., Kim, H.-.J., Lee, K., Park, M.-h., 2014. The geological CO2 storage capacity of the Jeju Basin, offshore southern Korea, estimated using the storage efficiency. Int. J. Greenhouse Gas Control 23, 22–29. https://doi.org/10.1016/j.ijggc.2014.01.014.

Leonte, M, Wang, B., Socolofsky, S.A., Mau, S., Breier, J.A., Kessler, J.D., 2018. Using Carbon Isotope Fractionation to Constrain the Extent of Methane Dissolution Into the Water Column Surrounding a Natural Hydrocarbon Gas Seep in the Northern Gulf of Mexico. Geochemistry, Geophysics, Geosystems 19. https://doi.org/10.1029/2018GC007705.

Li, J., White, P., Roche, B., Bull, J.M., Leighton, T.G., Davis, J.W., Fone, J.W., 2021. Acoustic and optical determination of bubble size distributions – Quantification of seabed gas emissions. Int. J. Greenhouse Gas Control. https://doi.org/10.1016/j.ijggc.2021.103313 this issue.

Lichtschlag, A., Haeckel, M., Olierook, D., Peel, K., Flohr, A., Pearce, C.R., Marieni, C., James, R.H., Marieni, C., Connelly, D.P., 2021. Impact of CO2 leakage from sub-seabed carbon dioxide storage on sediment and porewater geochemistry. Int. J. Greenhouse Gas Control. https://doi.org/10.1016/j.ijggc.2021.103352 this issue-a.

Lichtschlag, A., James, R.H., Stahl, H., Connelly, D., 2015. Effect of a controlled sub-seabed release of CO2 on the biogeochemistry of shallow marine sediments, their porewaters, and the overlying water column. Int. J. Greenhouse Gas Control 38, 80–92. https://doi.org/10.1016/j.ijggc.2014.10.008.

Linke, P., Haeckel, M.: Cruise Report POS518 - Baseline Study for the Environmental Monitoring of Subseafloor CO2 Storage Operations, Kiel, GEOMAR, 91, 2018.

Lichtschlag, A., Pearce, C.R, Suominen, M., Blackford, J., Borisov, S.M., Bull, J.M., de Beer, D., Dean, M., Flohr, A., Esposito, M., Gros, J., Haeckel, M., Huvenne, V.A.I., James, R.H., Koopmans, D., Linke, P., Mowlem, M., Omar, A.M., Schaap, A., Schmidt, M., Sommer, S., Strong, J.A., Connelly, D.P., n.d.. Suitability analysis and revised strategies for marine environmental carbon capture and storage (CCS) monitoring. International Journal of Greenhouse Gas Control. Submitted for publication.

Lv, Z., Chen, Z., Chen, X., Liang, J., Jiang, J., Loake, G.J., 2019. Effects of various feedstocks on isotope fractionation of biogas and microbial community structure during anaerobic digestion. Waste Manage. (Oxford) 84. https://doi.org/10.1016/j.wasman.2018.11.043, 211-219.

Mabon, L., Shackley, S., Bower-Bir, N., 2014. Perceptions of sub-seabed carbon dioxide storage in Scotland and implications for policy: a qualitative study. Mar. Policy 45, 9–15. https://doi.org/10.1016/j.marpol.2013.11.011.

Mabon, L., Shackley, S., Blackford, J.C., Stahl, H., Miller, A., 2015. Local perceptions of the QICS experimental offshore CO2 release: results from social science research. Int. J. Greenhouse Gas Control 38, 18–25. https://doi.org/10.1016/j.ijggc.2014.10.022.

Mabon, L., Kita, J., Xue, Z., 2017. Challenges for social impact assessment in coastal regions: a case study of the Tomakomai CCS Demonstration Project. Mar. Policy 83, 243–251. https://doi.org/10.1016/j.marpol.2017.06.015.

Matter, J.M., Stute, M., Snæbjörnsdottir, S.Ó., Oelkers, E.H., Gislason, S.R., Aradottir, E. S., Sigfusson, B., Gunnarsson, I., Sigurdardottir, H., Gunnlaugsson, E., Axelsson, G., Alfredsson, H.A., Wolff-Boenisch, D., Kiflom, M., Fernandez de la Reguera Taya, D., Hall, J., Dideriksen, K., Broecker, W.S., 2016. Rapid carbon mineralization for permanent disposal of anthropogenic carbon dioxide emissions. Science 352, 1312–1314. https://doi.org/10.1126/science.aad8132, 10.1126/science.aad8132.

Mayer, B., Humez, P., Bercker, V., Dalkhaa, C., Rock, L., Myrttinen, A., Barth, J.A.C., 2015. Assessing the usefulness of the isotopic composition of CO2 for leakage monitoring at CO2 storage sites: a review. Int. J. Greenhouse Gas Control 37, 46–60. https://doi.org/10.1016/j.ijggc.2015.02.021.

Miocic, J.M., Gilfillan, S.M.V., Roberts, J.J., Edlmann, K., McDermott, C.I., Haszeldine, R. S., 2016. Controls on CO2 storage security in natural reservoirs and implications for CO2 storage site selection. Int. J. Greenhouse Gas Control 51, 118–125. https://doi.org/10.1016/j.ijggc.2016.05.019.

Myers, M., La Force, T., White, C.M., Pejcic, B., Stalker, L., Ross, A.: Chemical Tracer Partition Coefficients for CCS. CSIRO Report # EP142797, 2012.

Myers, M., Stalker, L., Pejcic, B., Ross, A., 2013. Tracers - Past, present and future applications in CO2 geosequestration. Appl. Geochem. 30, 125–135. https://doi.org/10.1016/j.apgeochem.2012.06.001.

Myers, M.B., Roberts, J.J., White, C., Stalker, L., 2019. An experimental investigation into quantifying CO2 leakage in aqueous environments using chemical tracers. Chem. Geol. 511, 91–99. https://doi.org/10.1016/j.chemgeo.2019.02.033.

Myrttinen, A., Bercker, V., van Geldern, R., Würdemann, H., Morozova, D., Zimmer, M., Taubald, H., Blum, P., Barth, J.A.C., 2010. Carbon and oxygen isotope indications for CO2 behaviour after injection: first results from the Ketzin site (Germany). Int. J. Greenhouse Gas Control 4, 1000–1006. https://doi.org/10.1016/j.ijggc.2010.02.005.

Nelson, S.T., 2000. A simple, practical methodology for routine VSMOW/SLAP normalization of water samples analyzed by continuous flow methods. Rapid

Commun. Mass Spectrom. 14, 1044–1046. https://doi.org/10.1002/1097-0231(20000630)14:12<1044::AID-RCM987>3.0.CO;2-3.

Nimz, G., Hudson, G.: The use of noble gas isotopes for monitoring leakage of geologically stored CO2, Carbon Dioxide Capture for Storage in Deep Geologic Formations - Results from the CO2 Capture Project, 2, 1113–1128, 10.1016/B978-008044570-0/50152-5, 2005.

OSPAR, 2007. Amendment to 1992 OSPAR Convention. Convention for the Protection of the Marine Environment of the North-East Atlantic. https://www.ospar.org/convention/text.

Ozima, M., Podosek, F.A., 2002. Noble Gas Geochemistry. Cambridge University Press, Cambridge, New York, Melbourne. https://doi.org/10.1017/S0016756803258349, 2nd ed. xiv + 286 ppISBN 0 521 80366 7.3, Geological Magazine, 140, 616-617.

Poling, B.E., Prausnitz, J.M., O'Connell, J.P., 2001. The Properties of Gases and Liquids. J. Am. Chem. Soc. 27 edited by: Cox, K. R., Chapman, W. G., American Chemical Society, McGraw-Hill: New York, 6745-6745.

Reynolds, C.A., Menke, H., Andrew, M., Blunt, M.J., Krevor, S., 2017. Dynamic fluid connectivity during steady-state multiphase flow in a sandstone. Proc. Natl Acad. Sci. 114, 8187–8192. https://doi.org/10.1073/pnas.1702834114.

Rillard, J., Loisy, C., Le Roux, O., Cerepi, A., Garcia, B., Noirez, S., Rouchon, V., Delaplace, P., Willequet, O., Bertrand, C., 2015. The DEMO-CO2 project: a vadose zone CO2 and tracer leakage field experiment. Int. J. Greenhouse Gas Control 39, 302–317. https://doi.org/10.1016/j.ijggc.2015.04.012.

Ringrose, P.S., Meckel, T.A., 2019. Maturing global CO2 storage resources on offshore continental margins to achieve 2DS emissions reductions. Sci. Rep. 9, 17944. https://doi.org/10.1038/s41598-019-54363-z.

Roberts, J., Gilfillan, S., Stalker, L., Naylor, M., 2017. Geochemical tracers for monitoring offshore CO2 stores. Int. J. Greenhouse Gas Control 65, 218–234. https://doi.org/10.1016/j.ijggc.2017.07.021, 65218-23410.1016/j.ijggc.2017.07.021, 2017.

Roche, B., Bull, J.M., Marin-Moreno, H., Leighton, T.G., Falcon-Suarez, I.H., White, P.R., Provenzano, G., Tholen, M., Lichtschlag, A., Li, J., Fagetter, M., 2021. Time-lapse imaging of CO2 migration within near-surface sediments during a controlled sub-seabed release experiment. Int. J. Greenhouse Gas Control. https://doi.org/10.1016/j.ijggc.2021.103363 this issue.

Rock, L., Villegas, E.I., Becker, V., Dalkhaa, C., Humez, P., Nightingale, M., Shevalier, M., Mayer, B., Zhang, G., 2014. Investigation of Natural Tracers for MMV at the Quest Carbon Capture and Storage Project. Alberta, Canada, Energy Procedia 63, 4191–4198. https://doi.org/10.1016/j.egypro.2014.11.452.

Romanak, K.D., Bennett, P.C., Yang, C., Hovorka, S.D., 2012. Process-based approach to CO2 leakage detection by vadose zone gas monitoring at geologic CO2 storage sites. Geophys. Res. Lett. 39 https://doi.org/10.1029/2012 gl052426, 10.1029/2012 gl052426.

Romanak, K.D., Wolaver, B., Yang, C., Sherk, G.W., Dale, J., Dobeck, L.M., Spangler, L. H., 2014. Process-based soil gas leakage assessment at the Kerr Farm: comparison of results to leakage proxies at ZERT and Mt. Etna. Int. J. Greenhouse Gas Control 30, 42–57. https://doi.org/10.1016/j.ijggc.2014.08.008.

Schaap, A., Koopmans, D., Holtappels, M., Dewar, M., Arundell, M., Papadimitriou, S., Hanz, R., Monk, S., Mowlem, M., Loucaides, S., 2021. Quantification of a subsea CO2 release with lab-on-chip sensors measuring benthic gradients. Int. J. Greenhouse Gas Control. https://doi.org/10.1016/j.ijggc.2021.103427 this issue.

Schacht, U., Jenkins, C., 2014. Soil gas monitoring of the Otway Project demonstration site in SE Victoria, Australia. Int. J. Greenhouse Gas Control 24, 14–29. https://doi.org/10.1016/j.ijggc.2014.02.007.

Schmidt, M.: RV POSEIDON Fahrtbericht /Cruise Report POS534 Leg 1: kiel (Germany) - Aberdeen (United Kingdom) 01.05. -22.05.2019 Leg 2: aberdeen (United Kingdom) - Bremerhaven (Germany), 23.05. -29.05.2019, GEOMAR Helmholtz-Zentrum für Ozeanforschung, Kiel, Germany, 51, 2019.

Serno, S., Johnson, G., La Force, T., Ennis-King, J., Haese, R.R., Boreham, C., Paterson, L., Freifeld, B., Cook, P.J., Kirste, D., Haszeldine, R.S., Gilfillan, S., 2016. Using oxygen isotopes to quantitatively assess residual CO2 saturation during the CO2CRC Otway Stage 2B Extension residual saturation test. Int. J. Greenhouse Gas Control 52, 73–83. https://doi.org/10.1016/j.ijggc.2016.06.019, 10.1016/j.ijggc.2016.06.019.

Shell, 2015. Storage Development Plan - Peterhead CCS Project. Shell UK Limited 2015. https://www.gov.uk/government/uploads/system/uploads/attachment_data/file/531016/DECC_Ready_-_KKD_11.128_Storage_Development_Plan.pdf.

Shevalier, M., Dalkhaa, C., Humez, P., Mayer, B., Becker, V., Nightingale, M., Rock, L., Zhang, G., 2014. Coupling of TOUGHREACT-Geochemist Workbench (GWB) for modeling changes in the isotopic composition of CO2 leaking from a CCS storage reservoir. Energy Procedia 63, 3751–3760. https://doi.org/10.1016/j.egypro.2014.11.404, 10.1016/j.egypro.2014.11.404.

Socolofsky, S.: Texas A&M Oilspill Calculator (TAMOC) modeling suite for subsea spills, Proceedings of the Thirty-Eighth AMOP Technical Seminar (Environment Canada, Ottawa), 153-168, 2015.

Soltanian, M.R., Amooie, M.A., Cole, D., Graham, D., Pfiffner, S., Phelps, T., Moortgat, J., 2018. Transport of perfluorocarbon tracers in the Cranfield Geological Carbon Sequestration Project. Greenhouse Gas Sci Technol 650–671, 10.1002/ghg.1786.

Stalker, L., Boreham, C., Underschultz, J., Freifeld, B., Perkins, E., Schacht, U., Sharma, S., 2015. Application of tracers to measure, monitor and verify breakthrough of sequestered CO2 at the CO2CRC Otway Project, Victoria, Australia. Chem. Geol. 399, 2–19. https://doi.org/10.1016/j.chemgeo.2014.12.006.

Stanley, R.H.R., Jenkins, W.J., 2013. Noble Gases in Seawater as Tracers for Physical and Biogeochemical Ocean Processes. In: Burnard, P. (Ed.), The Noble Gases as Geochemical Tracers. Springer Berlin Heidelberg, Berlin, Heidelberg, pp. 55–79.

Tanhua, T., Olsson, K.A., Fogelqvist, E., 2004. A first study of SF6 as a transient tracer in the Southern Ocean. Deep-Sea Research II 51, 2683–2699. https://doi.org/10.1016/j.dsr2.2001.02.001.

Taylor, P., Stahl, H., Vardy, M.E., Bull, J.M., Akhurst, M., Hauton, C., James, R.H., Lichtschlag, A., Long, D., Aleynik, D., Toberman, M., Naylor, M., Connelly, D., Smith, D., Sayer, M.D.J., Widdicombe, S., Wright, I.C., Blackford, J., 2015. A novel sub-seabed CO2 release experiment informing monitoring and impact assessment for geological carbon storage. Int. J. Greenhouse Gas Control 38, 3–17. https://doi.org/10.1016/j.ijggc.2014.09.007.

Tong, F., Niemi, A., Yang, Z., Fagerlund, F., Licha, T., Sauter, M., 2013. A Numerical Model of Tracer Transport in a Non-isothermal Two-Phase Flow System for Geological Storage Characterization. Transp. Porous Media 98, 173–192. https://doi.org/10.1007/s11242-013-0138-x.

Vogel, J.C., Grootes, P.M., Mook, W.G.: Isotopic fractionation between gaseous and dissolved carbon dioxide, Zeitschrift für Physik A Hadrons and nuclei, 230, 225–238, 10.1007/BF01394688, 1970.

Van der Meer, L.G.H., 2013. 13 - The K12-B CO2 injection project in the Netherlands. Geological Storage of Carbon Dioxide (CO2). Woodhead Publishing, pp. 301–332. https://doi.org/10.1533/9780857097279.3.301.

Vandeweijer, V., van der Meer, B., Hofstee, C., Mulders, F., D'Hoore, D., Graven, H., 2011. Monitoring the CO2 injection site: K12-B. Energy Procedia (4), 5471–5478. https://doi.org/10.1016/j.egypro.2011.02.532.

Vangkilde-Pederson, T., 2009. D16 WP2 Report: EU GeoCapacity - Assessing European Capacity for Geological Storage of Carbon Dioxide. GeoCapacity Project. http://www.geology.cz/geocapacity/publications/D16%20WP2%20Report%20storage%20capacity-red.pdf.

White, S.N., Brewer, P.G., Peltzer, E.T., 2006. Determination of gas bubble fractionation rates in the deep ocean by laser Raman spectroscopy. Mar. Chem. 99, 12–23. https://doi.org/10.1016/j.marchem.2004.10.006.

Zeebe, R.E., Wolf-Gladrow, D.A., 2001. CO_2 in seawater: equilibrium, Kinetics, Isotopes, 346 pp. Elsevier Oceanography Series. edited by: Halpern, D.

Zhang, J., Quay, P.D., Wilbur, D.O., 1995. Carbon isotope fractionation during gas-water exchange and dissolution of CO2. Geochim. Cosmochim. Acta 59, 107–114. https://doi.org/10.1016/0016-7037(95)91550-D.

Zhong, L., Amonette, J.E., Mitroshkov, A.V., Olsen, K.B., 2014. Transport of perfluorocarbon tracers and carbon dioxide in sediment columns - Evaluating the application of PFC tracers for CO2 leakage detection. Appl. Geochem. 45, 25–32. https://doi.org/10.1016/j.apgeochem.2014.02.016.

Zhu, H., Liu, Q., Deng, J., Wang, G., Xiao, X., Jiang, Z., Zhang, D., 2011. Pressure and temperature preservation techniques for gas-hydrate-bearing sediments sampling. Energy 36, 4542–4551. https://doi.org/10.1016/j.energy.2011.03.053.